Available online at www.sciencedirect.com
SCIENCE DIRECT
Geochimica et Cosmochimica Acta 70 (2006) 871–890
Geochimica
www.elsevier.com/locate/gca

Do Archean chemical sediments record ancient seawater rare earth element patterns?

Karen H. Johannesson [a,*], Doyle L. Hawkins Jr. [b], Alejandra Cortés [c]

[a] Department of Earth and Environmental Sciences, The University of Texas at Arlington, Arlington, TX 76019-0049, USA
[b] Department of Mathematics, The University of Texas at Arlington, Arlington, TX 76019-0408, USA
[c] Instituto de Geofísica, Universidad Nacional Autónoma de México, 04510 México, DF, Mexico

Received 20 April 2005; accepted in revised form 21 October 2005

Abstract

Rare earth elements (REE) concentrations of Archean and Proterozoic chemical sediments are commonly used as proxies to study secular trends in the geochemistry of Precambrian seawater. In addition, similarities in the REE signatures of Archean chemical sediments and modern seawater have led researchers to argue that some Archean rocks originated as biochemical precipitates (i.e., microbial carbonates) in shallow marine (e.g., peritidal) environments. However, terrestrial waters, including river water and groundwater, also commonly exhibit REE fractionation patterns that resemble modern seawater. Here, we present the seawater-like REE data for groundwaters from central México as additional evidence that these patterns are not unique to the marine environment. The shale-normalized REE patterns of the groundwaters are compared to those of modern seawater (open ocean and nearshore), Holocene reefal microbial carbonates and corals, and Archean chemical sediments using statistical means (i.e., ANOVA and Wilcoxon analyses) in order to quantify the similarities and/or differences in the REE patterns. Shale-normalized (SN) Ce anomalies and measures of REE fractionation [i.e., $(La/Yb)_{SN}$, $(Pr/Yb)_{SN}$, $(Nd/Yb)_{SN}$, and $(Gd/Yb)_{SN}$] of the central México groundwater samples are statistically indistinguishable from those of modern seawater. Moreover, except for differences in the Ce anomalies, which are lacking in Archean chemical sediments, the REE patterns of the central México groundwaters are also statistically similar to REE patterns of Archean chemical sediments, especially those of the 3.45 Ga Strelley Pool Chert. Consequently, we suggest that without additional information, it may be premature to unequivocally conclude that Archean chemical sediments record REE signatures of an Archean ocean.

1. Introduction

The origins of life on Earth and the potential that life exists, or existed sometime in the past, on other planets in our solar system (e.g., Mars) is of fundamental interest to Earth and planetary scientists, as well as society as a whole (e.g., Urey, 1952; Miller, 1953; Barghoorn and Schopf, 1966; McKay et al., 1996). As a consequence, significant efforts have focused on understanding the origins of Early Archean rocks exposed in Greenland and Western Australia (3.45 Ga rocks of the Warrawoona Group of the Pilbara Craton, Western Australia; 3.7 Ga Isua Greenstone Belt of southwestern Greenland; 3.8 Ga rocks from Akilia Island off the Greenland coast) as these rocks comprise the oldest yet identified on the Earth's surface and may contain evidence of early life. For example, a variety of geologic features identified within, and geochemical data collected from these rocks have been interpreted by some researchers as the earliest evidence of life on Earth, whereas others have argued strongly against the presence of any biogenic signatures in these rocks (e.g., Walter et al., 1980; Schopf and Packer, 1987; Rosing, 1999; Fedo and Whitehouse, 2002). Arguments for preservation of biogenic indicators in these Archean rocks are based on sedimentary structures (e.g., stromatolitic bedforms), microscopic features that resemble, to a degree, bacteria, and perhaps most convincing, isotopically light signatures of reduced carbon within these rocks (Schopf, 1993; Mojzsis et al., 1996). However, other researchers dismiss the reported

* Corresponding author.
E-mail address: kjohanne@uta.edu (K.H. Johannesson).

0016-7037/$ - see front matter © 2005 Elsevier Inc. All rights reserved.
doi:10.1016/j.gca.2005.10.013

microscopic forms as not actually resembling microbes, argue that the light carbon is of hydrothermal and/or volcanic origin, and provide strong evidence that at least some of the rocks in question are not of sedimentary origin, but instead are metasomatized, ultramafic igneous rocks (Brasier et al., 2002; Fedo and Whitehouse, 2002). Recently, shale-normalized rare earth element (REE) patterns of some Archean chemical sediments, including rocks of the Warrawoona Group in Western Australia and the Isua Greenstone Belt of Greenland, have been cited as evidence for their formation as biochemical precipitates (e.g., microbialites) within shallow marine environments (Kamber and Webb, 2001; Van Kranendonk et al., 2003; Bolhar et al., 2004), thus supporting the presence of early microbial life forms.

In addition to their use in the study of the petrogenesis of igneous rocks and for tracing circulation and mixing of oceanic water masses (Hanson, 1980; Piepgras and Wasserburg, 1987), REEs have been employed as proxies for investigating secular trends in ocean chemistry through geologic time. It is generally agreed, for example, that the REE concentrations of Archean and Proterozoic banded iron formations (BIF) provide a record of paleo-ocean chemistry. Specifically, the positive shale-normalized Eu anomalies and lack of Ce anomalies that characterize BIF's are thought to reflect the importance of high-temperature (>250 °C) hydrothermal discharges along the seafloor (i.e., so-called "mantle-flux") and the substantially lower P_{O_2} levels, respectively, in the Archean and early Proterozoic oceans and atmosphere (Derry and Jacobsen, 1990; Shimizu et al., 1990; Danielson et al., 1992; Bau and Möller, 1993). Other investigators have focused on the REE signatures of phosphorites and biogenic apatite as tools for studying ancient seawater chemistry, and based on these studies, have suggested that the relative distribution of REEs in seawater from the geologic past differed from that of the modern ocean (McArthur and Walsh, 1984/1985; Grandjean et al., 1987; Wright et al., 1987; Lécuyer et al., 2004). It is important to stress, however, that to a large degree most paleo-seawater proxies (e.g., biogenic "skeletal" carbonates and phosphates, hydrogenous Fe–Mn minerals, and abiotic carbonates, phosphates and silicates) fail to preserve the REE distributions of the ancient oceans within which they formed (Shields and Webb, 2004). These proxies fail for a number of reasons including post-diagenetic mobilization of REEs, fractionation of REEs during precipitation/uptake, and/or because they exhibit exceedingly low REE concentrations that are easily contaminated by exogenous sources (Palmer, 1985; Elderfield and Pagett, 1986; Palmer and Elderfield, 1986; Sholkovitz and Shen, 1995; Bau et al., 1996; Reynard et al., 1999; Shields and Stille, 2001). Nonetheless, Webb and Kamber (2000) suggest that microbial carbonates may be especially robust proxies for evaluating paleo-seawater chemistry. These investigators demonstrate, for example, that Holocene reefal microbialites from the Great Barrier Reef (GBR) incorporate REEs from ambient seawater at substantially higher concentrations than other biogeochemical precipitates. Furthermore, based on calculated solid–liquid partitioning coefficients for REEs in these microbialite samples, which are relatively uniform across the REE series, Webb and Kamber (2000) argue that REEs are not fractionated from seawater during precipitation of microbial carbonates. More recently, Wyndham et al. (2004) suggest that REE fractionation patterns of corals may also provide a useful proxy for biological processes occurring in nearshore marine environments.

Despite these observations, it is important to underscore that terrestrial waters also commonly display REE patterns that broadly resemble those of modern seawater (e.g., Dia et al., 2000; Leybourne et al., 2000; Négrel et al., 2000). Furthermore, the heavy REE (HREE) enriched, shale-normalized REE patterns that characterize modern seawater originate, in part, during chemical weathering of the continents and from the effects of solution and surface complexation reaction on dissolved REEs during transport to the oceans in rivers and estuaries (i.e., Hoyle et al., 1984; Goldstein and Jacobsen, 1988; Elderfield et al., 1990; Sholkovitz, 1995; Byrne and Liu, 1998). In this contribution, we present REE data and shale-normalized fractionation patterns for groundwaters from central México that also closely resemble those of modern seawater. Using these groundwaters as examples of terrestrial waters with seawater-like REE patterns, we apply statistical techniques to more quantitatively examine the similarities and differences between REE patterns of the groundwaters, modern seawater, and Archean chemical sediments.

2. Background

2.1. Rare earth element fractionation patterns of modern seawater

Perhaps the two most noted features that characterize input-normalized REE fractionation patterns of modern seawater are the enrichments in HREEs compared to light REEs (LREE) and the negative Ce anomalies (Elderfield and Greaves, 1982; Elderfield, 1988; Bertram and Elderfield, 1993; Fig. 1). In addition to these characteristics, input-normalized REE fractionation patterns of modern seawater also exhibit a number of subtle features including elevated, normalized La values compared to other LREEs (e.g., Pr and Nd), variable Eu anomalies, positive Gd anomalies, and substantial Y/Ho ratios, commonly referred to as Y-anomalies (Figs. 1 and 2; Zhang et al., 1994; Bau et al., 1995; Nozaki et al., 1997). Input-normalized REE patterns (e.g., Fig. 1) represent the relative concentration of each REE in the sample (i.e., seawater) as compared to their chief source concentration, which in the case of the oceans is detrital material produced from weathering of continental crust (e.g., Taylor and McLennan, 1985; Goldstein and Jacobsen, 1987). Other less significant sources of REEs to modern oceans include atmospheric deposition of dust and aerosols originating from continental regions, as well as hydrothermal inputs

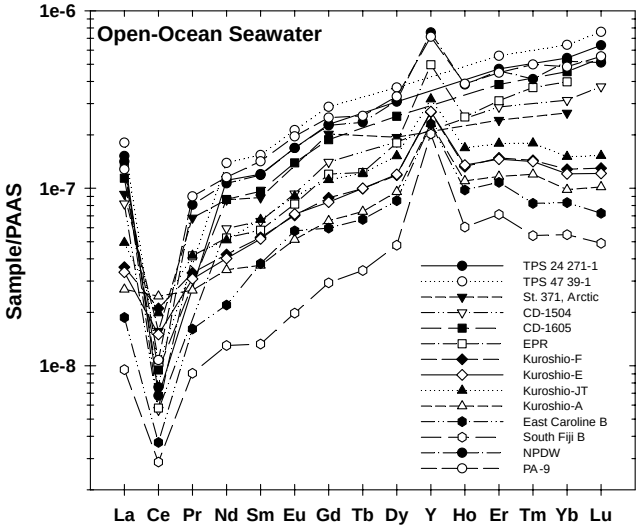

Fig. 1. Shale-normalized REE + Y patterns of open-ocean seawater sample using the shale composite Post Archean Australian Shale (PAAS) of Nance and Taylor (1976). Data are from: Piepgras and Jacobsen (1992), TPA 24 271-1 average of 1194 and 2000 m depths, TPS 47 39-1 average of 1249 and 2692 m depths; Westerlund and Öhman (1992), Station 371 average of 1000 and 2100 m depths; Bertram and Elderfield (1993), CD-1504 average of 1000 and 2100 m depths, CD-1605 is 2500 m depth sample; Möller et al. (1994) and Bau et al. (1995), average of 1000, 1200, 1500, 1600, 1800, and 2000 m depth; Nozaki and Zhang (1995), Kuroshio samples; Zhang and Nozaki (1996), East Caroline and South Fiji Basins; Nozaki and Alibo (2003), Station PA-9 average of 994, 1981, and 2716 m depths. Values for PAAS (in ppm) for Y and the REEs are: Y (27), La (38), Ce (80), Pr (8.9), Nd (32), Sm (5.6), Eu (1.1), Gd (4.7), Tb (0.77), Dy (4.4), Ho (1.0), Er (2.9), Tm (0.4), Yb (2.8), and Lu (0.43; Nance and Taylor, 1976).

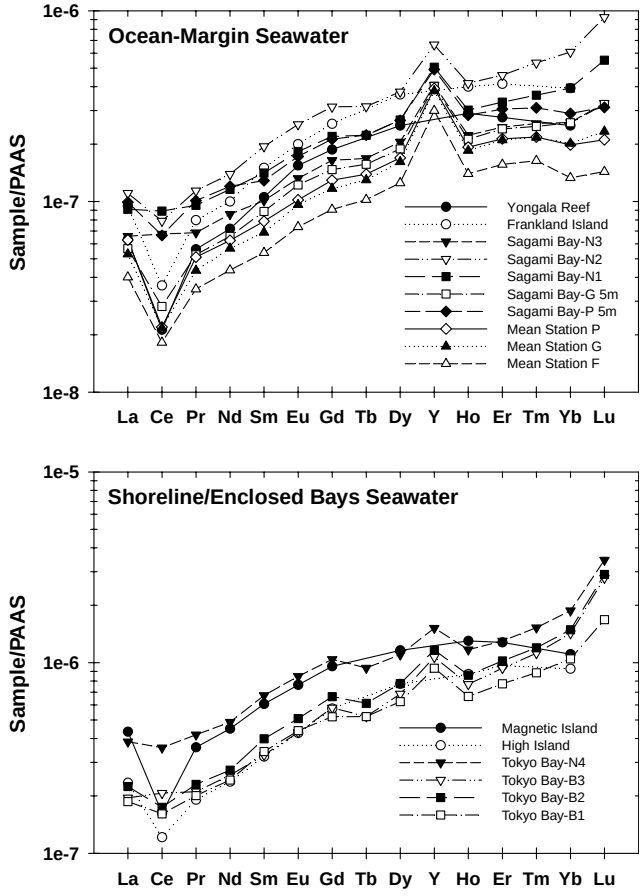

Fig. 2. Shale-normalized (i.e., PAAS) REE + Y patterns of ocean-margin and shoreline/enclosed bay seawater. Surface samples from Tokyo Bay and Sagami Bay/trough (Japan) N1, N2, N3, G, and P are from Nozaki and Zhang (1995). Stations P, G, and F (Zhang and Nozaki, 1998) are the average values of the upper 200 m of the water column from along the slope of the Sagami Bay/trough. The Magnetic, High, and Frankland Island and Yongala Reef seawater samples are from Wyndham et al. (2004). Magnetic and High Islands seawater samples are included with the Tokyo Bay samples (shoreline/enclosed bays) because of their proximity to the shoreline, whereas the Yongala Reef and Frankland Island seawater samples are included with the ocean-margin samples of the Sagami Bay/trough owing to their greater distance from the shoreline (Wyndham et al., 2004).

along the seabed (e.g., mid-ocean ridges; Elderfield and Greaves, 1982; Klinkhammer et al., 1983; Goldstein and Jacobsen, 1987; Sholkovitz et al., 1993). Because the composition of the upper continental crust is closely approximated by the composition of shales (Taylor, 1964; Taylor and McLennan, 1985), average shale composites, such as PAAS, are commonly used for input-normalization of dissolved REE concentrations in modern seawater (Elderfield, 1988).

Shale-normalized REE patterns (normalized to Post Archean Australian Shale, PAAS; Nance and Taylor, 1976) for open-ocean and near-shore seawater are presented in Figs. 1 and 2, respectively. The most obvious differences between the near-shore and open-ocean seawater samples are the higher REE concentrations and smaller Ce-anomalies and Y/Ho ratios of near-shore seawater (Table 1). The fact that REE fractionation patterns for seawater are not flat (i.e., shale-like) demonstrates that dissolved REEs in the oceans are fractionated with respect to their chief source, the upper continental crust. The presence of negative Ce anomalies (Fig. 1 and Table 1) reflects abiotic and biologically mediated oxidation of Ce^{3+} to Ce^{4+}, and subsequent removal of markedly less soluble tetravalent Ce from solution (Moffett, 1990, 1994; Sholkovitz and Schneider, 1991; DeCarlo et al., 1998). The HREE enrichment that characterizes modern seawater reflects competition between solution and surface complexation reactions, whereby formation of strong aqueous complexes with carbonate ions preferentially stabilizes HREEs in solution, lowering the activity of the free metal ion (e.g., Yb^{3+}), and thus inhibiting surface complexation of the HREEs compared to the LREEs (Cantrell and Byrne, 1987; Byrne and Kim, 1990; Koeppenkastrop and DeCarlo, 1992, 1993; Quinn et al., 2004). These processes are also known to be important in rivers and estuaries as the dissolved REE fraction delivered to the oceans via rivers commonly exhibits substantial enrichments in HREEs (Hoyle et al., 1984; Goldstein and Jacobsen, 1988; Elderfield et al., 1990; Sholkovitz, 1995; Byrne and Liu, 1998). Positive Eu anomalies, which are uncommon in seawater, are generally attributed to input from hydrothermal discharges along mid-ocean ridges (Klinkhammer et al., 1983, 1994).

Table 1
Shale-normalized Ce, Pr, and Gd anomalies, molal Y/Ho ratios, and shale-normalized La/Yb, Pr/Yb, Nd/Yb, and Gd/Yb ratios for selected analyses of modern seawater

	Ce/Ce^*	Pr/Pr^*	Gd/Gd^*	Y/Ho	La/Yb	Pr/Yb	Nd/Yb	Gd/Yb
Open-ocean								
TPS 24 271-1					0.28		0.20	0.42
TPS 47 39-1					0.28		0.22	0.45
CD-1504					0.26		0.19	0.45
CD-1605					0.25		0.19	0.41
Arctic St. 371	0.19	1.34			0.35	0.26	0.32	0.76
East Pacific Rise	0.07	1.43	1.19	98.7	0.34	0.10	0.13	0.30
Kuroshio-F	0.61	1.05	1.05	102	0.28	0.26	0.33	0.69
Kuroshio-E	0.47	1.12	1.00	100	0.28	0.26	0.33	0.69
Kuroshio-JT	0.43	1.18	1.08	94.2	0.33	0.28	0.34	0.74
Kuroshio-A	0.92	0.90	1.06	105	0.27	0.27	0.35	0.67
East Caroline B	0.21	1.25	1.04	118	0.23	0.19	0.26	0.72
South Fiji B	0.31	1.14	1.07	168	0.17	0.17	0.24	0.54
NPDW	0.07	1.41	1.15	98.4	0.27	0.16	0.21	0.44
PA-9	0.10	1.43	1.15	92.2	0.26	0.19	0.24	0.52
Mean	0.34	1.23	1.09	108	0.28	0.15	0.25	0.56
SD	0.27	0.18	0.06	23.4	0.04	0.11	0.07	0.15
Median	0.26	1.22	1.07	100	0.28	0.18	0.24	0.53
Enclosed Bays (& shoreline)								
Magnetic Island	0.41	1.17			0.39	0.32	0.41	0.86
High Island	0.57	1.06			0.25	0.21	0.26	0.62
Tokyo Bay-N4	0.89	0.99	1.22	65.0	0.21	0.22	0.26	0.55
Tokyo Bay-B3	1.02	0.91	1.27	69.5	0.14	0.15	0.18	0.41
Tokyo Bay-B2	0.77	1.03	1.23	67.9	0.15	0.15	0.18	0.45
Tokyo Bay-B1	0.83	1.00	1.13	70.4	0.18	0.19	0.23	0.50
Mean	0.75	1.03	1.21	68.2	0.22	0.21	0.25	0.56
SD	0.22	0.09	0.06	2.38	0.09	0.06	0.08	0.17
Median	0.80	1.01	1.22	68.7	0.16	0.20	0.24	0.53
Ocean-margin (coastal)								
Yongala Island	0.36	1.21			0.25	0.22	0.29	0.75
Frankland Island	0.42	1.17			0.24	0.20	0.25	0.65
Sagami Bay-N3	1.00	0.90	1.13	91.8	0.25	0.26	0.33	0.63
Sagami Bay-N2	0.70	1.04	1.14	79.8	0.18	0.19	0.23	0.52
Sagami Bay-N1	0.95	0.93	1.12	84.1	0.23	0.24	0.29	0.56
Station G 5 m	0.52	1.12	1.09	95.1	0.22	0.20	0.25	0.57
Station P 5 m	0.66	1.08	1.11	87.1	0.34	0.35	0.42	0.73
Station P mean	0.38	1.21	1.09	102	0.32	0.26	0.32	0.65
Station G mean	0.45	1.11	1.07	103	0.26	0.22	0.28	0.58
Station F mean	0.49	1.12	1.05	107	0.30	0.26	0.33	0.68
Mean	0.59	1.09	1.10	93.7	0.26	0.24	0.30	0.63
SD	0.23	0.11	0.03	9.80	0.05	0.05	0.05	0.08
Median	0.50	1.11	1.10	93.5	0.25	0.23	0.29	0.64
Overalls								
Mean	0.48	1.13	1.12	95.2	0.26	0.22	0.27	0.58
SD	0.30	0.16	0.07	21.9	0.06	0.06	0.07	0.13
Median	0.44	1.12	1.11	95.1	0.26	0.22	0.26	0.57

$Ce/Ce^* = [Ce/(0.5La + 0.5Pr)]_{SN}$.
$Pr/Pr^* = [Pr/(0.5Ce + 0.5Nd)]_{SN}$.
$Gd/Gd^* = [Gd/(0.33Sm + 0.67Tb)]_{SN}$.
SN = Post Archean Australian Shale (PAAS; Nance and Taylor, 1976).

The more subtle features recorded by shale-normalized REE patterns of modern seawater arise, in part, from the progressive filling of the 4f electron shell across the REE series, which imparts small but important differences in the chemical properties of the REEs. Enrichments in La compared to other LREEs (i.e., Pr and Nd), for example, indicate greater stability of La in seawater, which is thought to reflect its empty 4f electron shell (Byrne and Kim, 1990; De Baar et al., 1991; Bolhar et al., 2004). Additionally, Gd owes its anomalous behavior to its half-filled

4f electron shell, which strongly affects solution and surface complexation of Gd relative to its nearest neighbors, Eu and Tb (Byrne and Kim, 1990; Kim et al., 1991; Byrne and Li, 1995; Byrne et al., 1996). As a consequence, shale-normalized patterns for modern seawater commonly exhibit positive La and Gd anomalies (Figs. 1 and 2).

Open-ocean seawater is also characterized by large, superchondritic Y/Ho ratios (Høgdahl et al., 1968; Zhang et al., 1994; Bau et al., 1995; Nozaki et al., 1997). Molal Y/Ho ratios for seawater samples analyzed by Nozaki et al. (1997), for example, range from ~80 to ~150, with a mean (±SD) of 108 ± 12 ($n = 93$). Similar molal Y/Ho ratios for seawater that range from 82 to 137 are reported by Bau (1996). By comparison, the molal Y/Ho ratio of crustal rocks, as well as chondrites, is remarkably uniform at ~48 to ~50 (Nozaki et al., 1997). The open-ocean seawater samples shown in Fig. 1 that have accompanying Y data exhibit molal Y/Ho ratios that range from 92 to 168 (mean ± SD = 108 ± 23; Table 1), whereas Y/Ho ratios for the ocean-margin seawater (Fig. 2) range from 80 to 107 (mean ± SD = 93.7 ± 9.8; Table 1). By comparison, the seawater samples collected closer to shore and within Tokyo Bay (i.e., shoreline/enclosed bays) have lower (i.e., more chondritic) Y/Ho ratios ranging from 65 to 70 (Table 1).

Because the ionic radii of Ho^{3+} and Y^{3+} are almost identical, both are expected to exhibit similar geochemical behavior in natural waters (e.g., Zhang et al., 1994; Nozaki et al., 1997). However, the fact that Y/Ho ratios are not constant in the oceans and vary with depth (Høgdahl et al., 1968; Nozaki et al., 1997) indicates that biogeochemical processes fractionate these trace elements. Since Høgdahl et al.'s initial observation, numerous investigators have sought to explain the mechanism or mechanisms responsible for the enrichments in seawater Y/Ho ratios. Differences in solution and surface complexation behavior, variable Y and Ho phosphate mineral solubilities, and fractionation during chemical weathering of continental source regions have all been advanced to explain the Y anomaly (Zhang et al., 1994; Bau et al., 1995; Bau, 1999; Nozaki et al., 1997; Bolhar et al., 2004).

Input-normalized enrichments or depletions of a given REE compared to its nearest neighbors in the lanthanide series are quantified by calculating ratios that compare the actual, shale-normalized value to the value predicted based on linear interpolation using neighboring REEs. Negative Ce anomalies, for example, have been quantified using $Ce/Ce^* = [3Ce/(2La + Nd)]_{SN}$, where SN indicates shale-normalized (Elderfield and Greaves, 1982). However, with the advent of analytical techniques that allow for measurement of all 14 naturally occurring REEs in water samples, such as inductively coupled plasma mass spectrometry (ICP-MS), Ce anomalies are now commonly calculated as $Ce/Ce^* = [Ce/(0.5La + 0.5Pr)]_{SN}$ (e.g., see Bau and Dulski, 1996). Here, we use the equation from Bau and Dulski (1996) to calculate Ce anomalies. We quantified the Pr anomaly (a measure of La enrichment; Bau and Dulski, 1996) using $Pr/Pr^* = [Pr/(0.5Ce + 0.5Nd)]_{SN}$ (Table 1). The Gd anomaly was calculated using $Gd/Gd^* = [Gd/(0.33Sm + 0.67Tb)]_{SN}$ (Webb and Kamber, 2000), whereas the Y anomaly was quantified as the molal Y/Ho ratio (Table 1; Nozaki et al., 1997). We also present shale-normalized La/Yb, Pr/Yb, Nd/Yb, and Gd/Yb ratios for open-ocean and near-shore seawater in Table 1 as measures of REE fractionation. Identical ratios are calculated below for Archean and Holocene chemical sediments, modern corals, and groundwaters from central México.

2.2. Fractionation patterns of chemical sediments

A number of recent studies discuss the similarities in shale-normalized REE patterns of chemical sediments and modern seawater, relying heavily on these similarities to reconstruct the paleo-environment within which the sediment formed (e.g., Kamber and Webb, 2001; Van Kranendonk et al., 2003; Bolhar et al., 2004, 2005; Kamber et al., 2004; Nothdurft et al., 2004). Initially, Webb and Kamber (2000) measured REE concentrations in Holocene reefal microbialites from the GBR and reported shale-normalized REE patterns for these carbonate rocks that resemble those of modern seawater. Specifically, the shale-normalized patterns of the microbialites exhibited enrichments in the HREEs compared to the LREEs, negative Ce anomalies, positive La anomalies, and small positive Gd anomalies (Webb and Kamber, 2000). Fig. 3 shows 10 of the 52 microbialite samples analyzed by these authors. The majority of the microbialites exhibit remarkably uniform shale-normalized REE patterns. The mean (±SD)

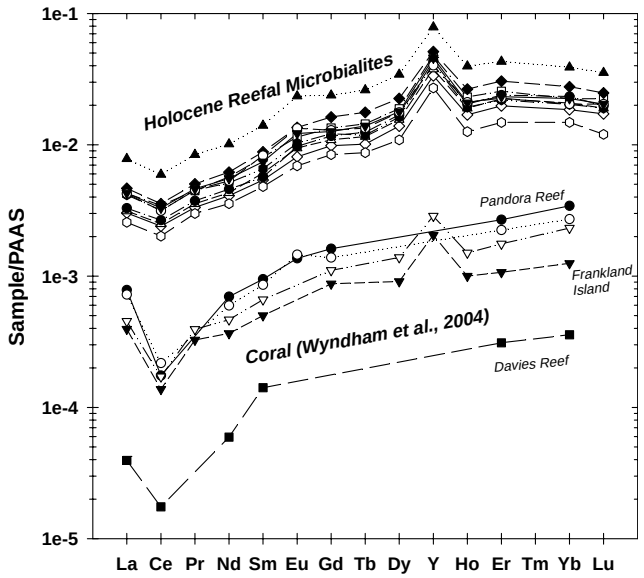

Fig. 3. Shale-normalized (i.e., PAAS) REE + Y patterns of Holocene reef microbialites from Webb and Kamber (2000) and modern reef coral from Wyndham et al. (2004). Holocene microbialite samples include H-1 m, H1-11 m (base), H1-12 m (top), H-2, H2-8 m (middle), H-9 m, H10-6 m (top), H10-9 m (base), H-19 m, and H-22 m from Table 1 of Webb and Kamber (2000).

shale-normalized Nd/Yb ratio for all 52 samples (i.e., 0.236 ± 0.026), for example, is identical to that for the 10 samples shown in Fig. 3 (0.236 ± 0.021; Table 2). The microbialite samples also have large positive Y/Ho ratios similar to seawater (i.e., molal Y/Ho $= 104 \pm 4.9$ for all 52 analyses; Webb and Kamber, 2000). The mean molal Y/Ho ratio (±SD) of the 10 samples presented in Table 2 and plotted in Fig. 3 is 106 ± 4.9. Modern coral from the GBR (Wyndham et al., 2004) have similar shale-normalized REE patterns to the microbialites, although their REE concentrations are approximately an order of magnitude lower (Fig. 3, Table 2).

Webb and Kamber (2000) argue that the similarity in shale-normalized REE patterns between the reefal microbialites and modern seawater indicates that the microbialites quantitatively incorporated REEs from ambient, shallow and oxygenated seawater during precipitation. Furthermore, the high REE contents of the microbialites compared to other seawater proxies (e.g., skeletal carbonates such as modern reef coral, Fig. 3), in addition to the uniform solid–liquid partition coefficients that these authors calculated for incorporation of REE into the microbialites (i.e., $K_D^{solid/liquid} = 295.6 \pm 30.2$; excluding Ce), further support their arguments and led them to hypothesize that microbialites are better proxies of paleoseawater chemistry than other proxies commonly in use. They conclude that ancient carbonate rocks (preferably limestones) that exhibit high REE concentrations and are not contaminated by continentally derived sediments, represent ancient microbial carbonates that have preserved the chemistry of the ancient seawater from which they precipitated (Webb and Kamber, 2000).

In a subsequent study of Late Archean stromatolitic carbonate rocks from South Africa, these same investigators provided additional evidence for their arguments. Shale-normalized REE patterns of presumed microbial carbonates from the 2.52 Ga Campbellrand carbonate platform (data not shown) mimic those of modern seawater by exhibiting positive La, Gd, and Y anomalies (Kamber and Webb, 2001). However, many carbonate rock samples of the Campbellrand exhibit shale-normalized enrichments in the LREEs compared to the HREEs (e.g., see Fig. 4 of Kamber and Webb, 2001). The shale-normalized Nd/Yb ratios of the Campbellrand carbonate rocks, for example, range from 0.37 to 2.19 (mean ± SD $= 0.95 \pm 0.62$). These authors argue that the ancient carbonate rocks of the Campbellrand platform preserve REE signatures of deep, anoxic waters of a Late Archean ocean. In such an Archean ocean, hydrothermal inputs along the seafloor were important and Fe(II) in the exhalants was not oxidized by the low P_{O_2} (i.e., anoxic) seawater. Hence, because Fe(II) was not oxidized, Fe(III) oxyhydroxides did not pre-

Table 2
Shale-normalized Ce, Pr, and Gd anomalies, molal Y/Ho ratios, and shale-normalized La/Yb, Pr/Yb, Nd/Yb, and Gd/Yb ratios for selected analyses of corals (Wyndham et al., 2004) and Holocene microbialites (Webb and Kamber, 2000) from the Great Barrier Reef

	Ce/Ce*	Pr/Pr*	Gd/Gd*	Y/Ho	La/Yb	Pr/Yb	Nd/Yb	Gd/Yb
Corals[a]								
Pandora Reef					0.23		0.2	0.47
Havannah Reef					0.27		0.22	0.51
Frankland Island	0.38	1.3		103	0.32	0.26	0.29	0.7
High Island	0.4	1.23		95.6	0.19	0.17	0.2	0.48
Davies Reef					0.11		0.17	
Mean	0.39	1.27		99.1	0.22	0.22	0.22	0.54
SD					0.08		0.05	0.11
Median	0.39	1.27		99.1	0.23	0.22	0.2	0.49
Holocene microbialites[b]								
H-1m	0.79	0.98	1.09	107	0.19	0.20	0.25	0.60
H1-11m base	0.73	1.03	1.10	100	0.17	0.18	0.22	0.59
H1-12m top	0.75	1.03	1.15	103	0.16	0.18	0.22	0.53
H-2m	0.73	1.05	1.08	103	0.20	0.22	0.26	0.61
H2-8m middle	0.75	1.04	1.12	103	0.15	0.17	0.21	0.53
H-9m	0.73	1.08	1.20	111	0.20	0.22	0.25	0.60
H10-6m top	0.72	1.08	1.13	112	0.17	0.20	0.24	0.57
H10-9m base	0.76	1.03	1.14	110	0.14	0.16	0.20	0.50
H-19m	0.72	1.07	1.10	99	0.21	0.22	0.26	0.63
H-22m	0.74	1.05	1.07	114	0.19	0.21	0.25	0.56
Mean	0.74	1.04	1.12	106	0.18	0.20	0.24	0.57
SD	0.02	0.03	0.04	4.93	0.02	0.02	0.02	0.04
Median	0.74	1.04	1.11	105	0.18	0.20	0.24	0.58

Composite shale used for normalization, SN, is PAAS (Nance and Taylor, 1976). Cerium, Pr, and Gd anomalies are calculated as discussed in text and Table 1. Because of the lack of Pr, Tb, and Y data for all but the Frankland and High Island coral samples, values for Ce/Ce*, Pr/Pr*, Y/Ho, and $(Pr/Yb)_{SN}$ could only be determined for these two samples.

[a] Wyndham et al. (2004).

[b] Webb and Kamber (2000).

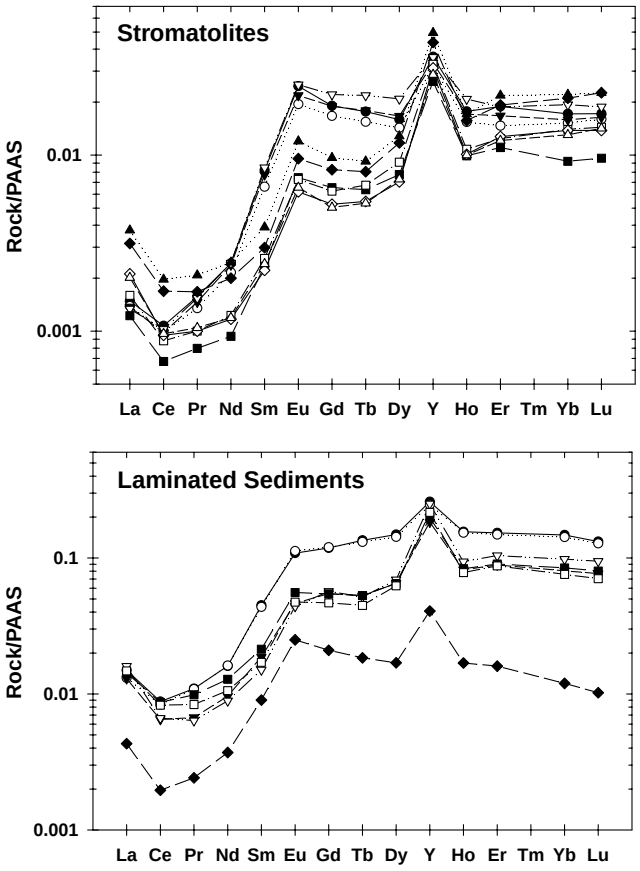

Fig. 4. Shale-normalized REE + Y patterns of stromatolitic and laminated sedimentary rock types of the Strelley Pool Chert of the Warrawoona Group, Pilbara Craton, Australia from Table 1 of Van Kranendonk et al. (2003). Despite the fact that PAAS is a composite of 23 analyses of shales younger than the Archean, PAAS was chosen for the current study in order to be consistent with other investigations of these and other Archean chemical sediments (i.e., Kamber and Webb, 2001; Van Kranendonk et al., 2003; Bolhar et al., 2004; Kamber et al., 2004).

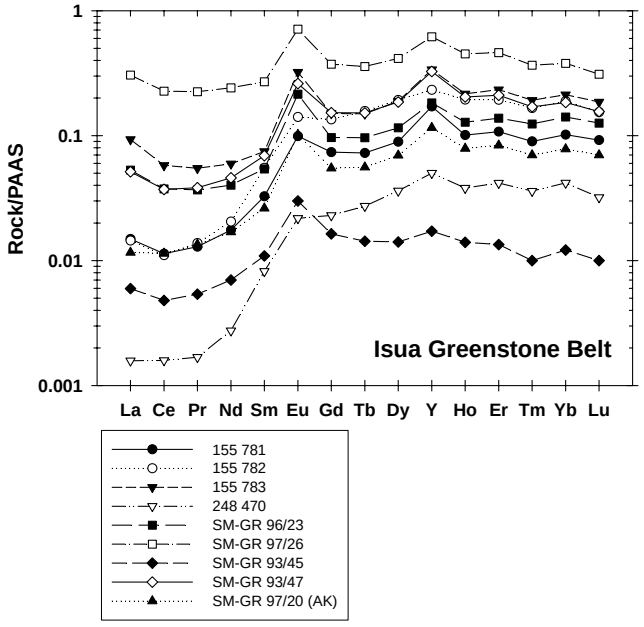

Fig. 5. Shale-normalized REE + Y patterns for presumed BIFs of the Isua Greenstone Belt, Greenland, and a sample from the nearby Akilia associated rocks. Data from Table 2 of Bolhar et al. (2004).

cipitate and thus REEs were not scavenged from solution by precipitating Fe(III) oxyhydroxides as occurs in the modern ocean (Kamber and Webb, 2001). More recently, these researchers report similar findings for Late Archean stromatolitic carbonates from Zimbabwe and Phanerozoic (Late Devonian) reefal carbonates of the Canning Basin in Western Australia (Kamber et al., 2004; Nothdurft et al., 2004). The Phanerozoic reefal carbonates of Western Australia's Canning Basin (data not shown) have shale-normalized REE signatures that suggest deposition in shallow, oxygenated seawater (see Fig. 5 of Nothdurft et al., 2004). The Late Archean stromatolites of Zimbabwe (data not shown) exhibit positive La and Gd anomalies, and large superchondritic Y/Ho ratios (see Figs. 3 and 4 of Kamber et al., 2004). However, many samples of these Archean chemical sediments are also enriched in the LREEs as demonstrated by their $(Nd/Yb)_{SN}$ ratios that range from 0.51 to 5.36 (mean $\pm$ SD $= 1.6 \pm 1.1$, $n = 16$). Kamber et al. (2004) argue that the LREE enrichment of the Archean stromatolitic carbonates from Zimbabwe reflects deposition in a restricted basin dominated by continental sources such as the local tonalite gneiss. It should be noted, however, that none of the near-shore seawater samples shown in Fig. 2 exhibit enrichments in the LREEs compared to the HREEs when normalized to shale including those from Tokyo Bay, whereas some natural terrestrial waters, including groundwaters from a shallow coastal aquifer, are indeed enriched in LREEs (see Smedley, 1991; Duncan and Shaw, 2003).

Van Kranendonk et al. (2003) investigated 3.45 Ga stromatolitic carbonate rocks (i.e., Strelley Pool Chert) of the Warrawoona Group from the Pilbara Craton of Western Australia. These authors present: (1) sedimentary evidence for the biogenicity of these Archean carbonate rocks; and (2) REE data as additional support for a shallow marine origin for these presumed microbial carbonates. The shale-normalized REE signatures of stromatolitic and laminated dolomitic rocks of the Strelley Pool Chert exhibit substantial depletions in LREEs compared to both middle REEs (MREE) and HREEs, possess positive La, Eu, and Y anomalies, and have either small or negligible Ce anomalies (Fig. 4; Van Kranendonk et al., 2003). The lack of significant negative Ce anomalies, a common feature of Archean chemical sediments, points towards anoxic conditions, the positive La anomalies and large Y/Ho ratios support deposition in shallow waters, and the positive Eu anomalies imply that input from hydrothermal sources (i.e., mantle-flux) was important during the formation of the Strelley Pool Chert (Table 3; Van Kranendonk et al., 2003). These authors conclude, based on interpreted primary sedimentary structures and the shale-normalized REE signatures that the carbonate rocks of the Strelley Pool Chert were precipitated from seawater as microbial carbonate sediments within a shallow, peritidal setting

Table 3
Shale-normalized Ce, Pr, and Gd anomalies, molal Y/Ho ratios, and shale-normalized La/Yb, Pr/Yb, Nd/Yb, and Gd/Yb ratios for rocks from the Isua Greenstone Belt and Akilia Island [SM-GR 97/20 (AK)], Greenland (Bolhar et al., 2004) and the Strelley Pool Chert, Western Australia (Van Kranendonk et al., 2003)

	Ce/Ce^*	Pr/Pr^*	Gd/Gd^*	Y/Ho	La/Yb	Pr/Yb	Nd/Yb	Gd/Yb
Isua Greenstone								
155 781	0.89	0.77	0.79	88.1	0.12	0.19	0.36	0.79
155 782	0.88	0.59	0.89	62.2	0.07	0.13	0.36	1.02
155 783	0.94	0.92	0.64	81.2	0.31	0.32	0.40	0.80
248 470	0.78	0.56	0.87	68.5	0.05	0.09	0.26	0.85
SM-GR 96/23	0.95	0.88	0.65	74.2	0.30	0.32	0.43	0.76
SM-GR 97/26	0.96	0.98	0.70	71.2	0.73	0.78	0.87	1.15
SM-GR 93/45	0.91	0.86	0.74	63.9	0.48	0.70	1.09	1.43
SM-GR 93/47	0.92	0.86	0.72	83.1	0.24	0.29	0.44	0.97
SM-GR 97/20 (AK)	0.95	0.85	0.70	76.1	0.16	0.24	0.38	0.80
Mean	0.91	0.81	0.74	74.3	0.27	0.34	0.51	0.95
SD	0.05	0.13	0.08	8.27	0.21	0.23	0.26	0.21
Median	0.92	0.86	0.72	74.2	0.24	0.29	0.40	0.85
Strelley Pool Chert—stromatolites								
2-9-11a	0.70	0.90	1.31	106	0.09	0.09	0.14	1.11
2-9-11b	0.73	0.86	1.33	109	0.09	0.09	0.14	1.10
2-9-11c	0.69	0.87	1.30	101	0.09	0.09	0.15	1.19
2-9-11d	0.71	0.89	1.27	90	0.07	0.08	0.13	1.14
2-9-23-a	0.67	0.99	1.30	138	0.13	0.09	0.10	0.71
2-9-23-b	0.68	0.95	1.16	158	0.11	0.07	0.09	0.45
SP177882-1/4	0.70	0.91	1.29	144	0.15	0.08	0.09	0.39
SP177882-2/4	0.61	0.95	1.20	161	0.15	0.07	0.08	0.38
SP177882-3/4	0.68	0.94	1.29	150	0.17	0.09	0.11	0.44
SP177882-4/4	0.63	0.97	1.16	149	0.15	0.08	0.09	0.39
Mean	0.68	0.92	1.26	131	0.12	0.08	0.11	0.73
SD	0.03	0.04	0.06	24.9	0.03	0.01	0.02	0.34
Median	0.68	0.92	1.29	141	0.12	0.08	0.11	0.58
Strelley Pool Chert—laminated sediments								
2-9-17a	0.68	0.88	1.13	86.2	0.10	0.07	0.11	0.80
2-9-17b	0.70	0.89	1.17	83.5	0.09	0.08	0.11	0.84
2-9-18a	0.66	0.83	1.32	117	0.16	0.08	0.12	0.68
2-9-18b	0.59	0.82	1.44	138	0.16	0.06	0.09	0.58
2-11-15a	0.72	0.92	1.28	124	0.17	0.12	0.15	0.64
2-11-15b	0.72	0.89	1.31	144	0.20	0.11	0.14	0.62
W2-9-14	0.58	0.85	1.37	125	0.36	0.20	0.31	1.75
Mean	0.66	0.87	1.29	117	0.18	0.10	0.15	0.85
SD	0.05	0.03	0.10	21.9	0.08	0.04	0.07	0.38
Median	0.68	0.88	1.31	124	0.16	0.08	0.12	0.68

See Table 1 for details.

(Van Kranendonk et al., 2003). They further suggest a modern coastal sabkha environment as an analog.

Appel (1983) followed by Bolhar et al. (2004) examined REE signatures in metamorphosed, early Archean rocks (~3.7 to 3.8 Ga) from south west Greenland. The latter investigators argue that "inferred" BIFs from the Isua Greenstone Belt have shale-normalized REE patterns reminiscent of seawater, whereas the granitoid gneisses of the nearby Akilia associated rocks have REE patterns that do not support a marine origin (Bolhar et al., 2004). It is important to mention that recent Fe isotope data support these conclusions although the Fe isotope data also suggest that some Akilia rocks are of sedimentary origin (Dauphas et al., 2004). Shale-normalized REE patterns of the inferred BIFs from the Isua Belt Greenstones (Fig. 5) are depleted in LREEs compared to HREEs, exhibit positive La, Eu, and Y anomalies, and do not possess negative Ce anomalies (Table 3; Bolhar et al., 2004). Except for one sample [i.e., 97/20(AK); Fig. 5; Table 3], rocks of the Akilia association have smooth, convex upward shale-normalized patterns between La and Nd (no La or Ce anomalies), both negative and positive Eu anomalies, and minor or no Y anomalies (data not shown). For example, molal Y/Ho ratios for Akilia association rocks range from 55.6 to 60.6 (mean $\pm$ SD $= 57.5 \pm 1.8$), whereas for the inferred BIFs from the Isua Greenstones, molal Y/Ho ratios range from 62 to 88, with a mean ($\pm$SD) of 74.3 ± 8.3 (Table 3;

Bolhar et al., 2004). Consequently, these researchers argue that although REE signatures of Isua Greenstone Belt rocks are consistent with their formation in seawater, those for rocks of the Akilia association indicate igneous origins.

3. Methods

3.1. Sample collection

Prior to sample collection, all sample bottles were rigorously cleaned using trace element clean procedures (see Johannesson and Hendry, 2000; Johannesson et al., 2004). All wells sampled within the States of Guanajuato and Querétaro, México (Fig. 6) are production wells used for water supply, and accordingly are pumped continuously. Consequently, waters from these wells are characteristic of the groundwater within the local, fractured rhyolite and mixed felsic volcanic and sedimentary rock aquifers (Johannesson et al., 2005), and do not represent stagnant waters from the well bores. At each well-head, groundwater was collected with a large, collapsible polyethylene container (previously cleaned identically to the sample bottles). The collected groundwater sample was then immediately filtered through 0.45 μm Gelman Sciences in-line groundwater filter capsules (polyether sulfone membrane) by drawing the groundwater from the collapsible polyethylene container through Teflon tubing (cleaned in the same fashion as the sample bottles) via a peristalic pump, and subsequently through the in-line filter capsule. Each individual sample bottle (1 L) was rinsed three times with the filtered groundwater sample to condition the bottle before the bottle was filled with the actual filtered groundwater sample. The filtered groundwater samples were then immediately acidified to pH < 2 with ultra pure nitric acid (Seastar Chemicals, subboiling, distilled in quartz), doubled bagged within clean plastic bags, and returned to the large poly box for transport back to the laboratory.

Fig. 6. Schematic map of México showing the location of the State of Guanajuato and the City of Querétaro in the neighboring State of Querétaro. Groundwater samples were collected in the vicinity of the city of León in Guanajuato and the city of Querétaro in Querétaro.

3.2. Groundwater REE analysis

Rare earth element and Y concentrations were determined by high resolution, magnetic sector inductively coupled plasma mass spectrometry (Finnigan MAT *Element* II) following methods discussed previously (e.g., Johannesson and Lyons, 1994, Stetzenbach et al., 1994; Field and Sherrell, 1998; Hodge et al., 1998; Tang and Johannesson, 2005). In brief, each water sample was introduced to the ICP-MS using a cross-flow nebulizer without preconcentration (Tang and Johannesson, 2005). The isotopes ^{89}Y, ^{139}La, ^{140}Ce, ^{142}Ce, ^{141}Pr, ^{143}Nd, ^{146}Nd, ^{148}Sm, ^{149}Sm, ^{152}Sm, ^{151}Eu, ^{153}Eu, ^{157}Gd, ^{158}Gd, ^{159}Tb, ^{161}Dy, ^{163}Dy, ^{164}Dy, ^{165}Ho, ^{166}Er, ^{167}Er, ^{169}Tm, ^{172}Yb, ^{173}Yb, ^{174}Yb, and ^{175}Lu were used to quantify Y and the REEs in the water samples (Stetzenbach et al., 1994; Hodge et al., 1998). Although, many of these REE (and Y) isotopes are free of isobaric interferences, it is advantageous, when possible, to monitor multiple isotopes of a particular element as an additional check of isobaric interferences (e.g., Hodge et al., 1998). Measured $YREEO^+/YREE^+$ ratios were ordinarily <1%, and for those that were >1%, appropriate corrections were made (Johannesson and Lyons, 1994, 1995; Stetzenbach et al., 1994; Johannesson et al., 1997; Shannon and Wood, 2005).

The ICP-MS was calibrated and the sample concentrations verified using a series of REE+Y calibration standards of known concentrations (0.1, 2, 10, 100, 250, 500, and 1000 ng/kg). The calibration standards were prepared from NIST traceable High Purity Standards (Charleston, SC). Check standards prepared from Perkin Elmer multielement solutions were analyzed regularly during the analysis to certify accuracy (e.g., Hodge et al., 1998). In addition, ^{115}In was added to each sample as an internal standard. Both the NIST Standard Reference Material (SRM) "Trace Elements in Water" No. 1643b and the National Research Council Canada (Ottawa, Ont., Canada) SRM for trace elements in river waters (SRLS-3) were routinely run during analysis as additional checks. Detection limits were in the low pmol/kg level for the REEs and Y (Table 4). Except for Eu, analytical precision of replicate analyses was typically better than 5% RSD (relative SD), and better than 1% RSD for Y, La, Ce, Nd, and Yb. Nevertheless, for Eu the precision was always better than 10% RSD.

3.3. Statistical analysis

To quantify similarities and/or differences between the shale-normalized REE patterns of modern seawater,

Table 4
Yttrium and rare earth element concentrations (pmol/kg) for groundwater samples from the León Valley in Guanajuato and the City of Querétaro, Querétaro in central México

	Y	La	Ce	Pr	Nd	Sm	Eu	Gd	Tb	Dy	Ho	Er	Tm	Yb	Lu
León Valley															
Lagunillas	45.4	5.78	4.62	1.09	3.73	0.79	0.59	2.99	0.32	1.71	0.50	1.90	0.31	2.62	0.43
Ciudad 33	180	28.6	5.65	2.40	19.9	9.52	4.77	20.4	1.07	5.82	1.34	4.95	0.90	6.85	1.55
Ciudad 35	73.5	8.67	4.88	1.68	8.27	4.89	2.92	13.7	0.85	3.40	0.74	2.91	0.75	4.12	0.71
Ciudad 41	74.5	13.2	4.39	2.57	11.0	3.29	1.33	4.84	0.57	3.35	0.73	2.56	0.30	2.37	0.36
Ciudad 46	723	21.9	26.9	4.70	21.5	8.87	3.63	13.5	4.93	35.8	15.4	28.6	4.09	25.2	3.39
Oriente 4	112	17.7	4.96	2.62	13.9	4.55	1.77	6.29	0.57	3.66	0.99	3.65	0.53	4.08	0.76
Sur 8	118	18.7	6.93	2.23	12.0	4.22	1.36	3.89	0.56	3.51	1.04	3.82	0.57	3.69	0.68
Sur 11	121	24.0	3.77	3.71	18.5	6.11	2.79	11.2	0.78	5.11	1.21	4.07	0.57	3.95	0.58
Turbio B-1	200	40.7	27.6	5.69	30.6	10.6	4.30	15.8	0.84	4.57	1.33	5.74	1.09	8.82	1.99
Turbio 12	202	23.7	4.08	3.43	15.2	5.84	1.94	5.80	0.81	6.43	1.81	6.58	1.04	7.41	1.24
Turbio 14	138	38.7	8.63	7.46	33.5	8.30	2.91	9.26	1.11	6.35	1.56	5.08	0.71	4.55	0.70
Querétaro															
Capilla 1Bis	72.0	5.94	3.23	0.84	2.92	1.50	0.49	1.40	0.29	1.84	0.65	2.60	0.51	3.28	0.65
Capilla 2	105	5.52	3.05	1.28	5.53	1.23	0.52	1.98	0.59	3.71	1.16	4.63	0.89	6.25	1.22
Capilla 3	42.1	4.70	4.41	0.82	2.89	0.61	0.25	0.94	0.19	0.93	0.29	1.16	0.18	0.99	0.25
Capilla 6	259	27.0	20.3	3.86	15.0	6.75	2.99	11.8	1.30	8.62	2.44	9.83	1.71	13.0	2.53
Juriquilla-UNAM	42.6	5.42	3.06	1.06	4.04	1.05	0.45	1.69	0.32	1.81	0.32	0.91	0.21	1.29	0.26
Chichimequillas 2	58.4	8.99	3.76	1.48	3.64	1.14	0.65	2.98	0.31	2.32	0.61	2.18	0.28	2.07	0.39
Lomas del Marques 1Bis	392	97.9	175	28.6	116	29.7	9.84	29.3	5.68	33.8	7.27	21.3	2.94	16.7	2.68
San Isidro Miranda	39.9	9.50	6.81	1.96	6.41	1.17	0.49	1.86	0.27	1.82	0.44	1.38	0.18	0.98	0.22
Salitre	990	22.4	4.75	3.34	19.4	8.60	4.02	16.5	3.89	34.0	11.1	45.0	7.48	47.7	8.91
Santa Rosa Jaurequi	69.7	6.53	1.79	1.22	4.54	1.46	0.60	2.21	0.44	2.32	0.59	2.74	0.36	2.49	0.44
Expositor 1	119	8.28	2.88	2.04	7.81	2.37	0.93	3.33	0.72	4.89	1.40	5.51	0.84	6.70	0.87
Pueblito 3	92.0	7.38	3.62	1.26	4.87	1.44	0.53	1.80	0.34	2.57	0.80	3.77	0.68	5.83	1.04
Virreyes	41.5	4.12	1.74	0.68	1.86	0.38	0.15	0.56	0.22	1.24	0.40	1.72	0.22	1.53	0.28
La Negreta	2700	58.0	10.3	18.4	96.9	34.1	14.5	55.2	13.8	114	32.1	119	20.4	147	25.5
San Miguelito	78.0	7.19	2.88	1.72	7.11	2.06	0.51	0.84	0.48	3.08	0.88	3.10	0.47	3.39	0.60
Alameda Park	109	5.83	3.73	1.41	5.05	1.39	0.38	0.80	0.59	3.35	1.26	6.36	1.49	16.3	4.26
Tlacote	120	14.5	17.0	3.21	13.4	3.65	1.13	3.04	0.85	5.09	1.36	4.60	0.65	4.76	0.80
Mompani	169	11.0	4.32	2.03	7.57	2.69	0.76	1.72	0.66	5.54	1.61	6.14	0.96	6.30	1.09
Field blank	1.03	0.86	1.96	0.23	0.23	0.07	0.057	0.29	0.051	0.24	0.015	0.021	0.034	0.01	0.01
Detection limit	0.39	0.35	0.22	0.089	0.59	0.64	0.94	1.6	0.19	0.4	0.04	0.17	0.15	0.26	0.06

modern reef coral, Holocene and Archean chemical sediments, and groundwater samples from central México (Tables 1–3 and 5), statistical methods were employed to evaluate the differences in REE patterns between the sampled populations. Values for Ce, Gd, and Y anomalies (Ce/Ce^*, Gd/Gd^*, and Y/Ho, respectively) and the degree of HREE enrichment as determined by $(La/Yb)_{SN}$, $(Pr/Yb)_{SN}$, $(Nd/Yb)_{SN}$, and $(Gd/Yb)_{SN}$ were compared for each sampled population (e.g., León groundwaters vs. open-ocean seawater, etc.). Both ANOVA and Wilcoxon analyses were performed. The Wilcoxon analysis was done as a guard against possibly highly non-normal data. For ANOVA, the null hypothesis for each comparison is that the mean values for the parameters being compared are equal, whereas for the Wilcoxon, the null hypothesis is that the median values are the same. The mean and median values for each parameter for the different sets of samples are listed in Tables 1–3 and 5. Differences between the means or medians were considered to be statistically significant using a familywise type I error rate of $\alpha = 0.05$, controlled using the Bonferroni procedure. Because there were seven parameters compared, this required $p < 0.05/7 = 0.0071$ to be declared significant.

4. Results

4.1. REE concentrations and fractionation in groundwaters of central México

Table 4 presents REE concentrations of groundwater samples collected from central México (Fig. 6). Groundwater pH ranges from 6.35 to 8.03 (mean ± SD = 7.64 ± 0.32; data not shown), and alkalinity, reported at HCO_3^-, ranges from 2.88 to 11.03 mmol/kg (mean ± SD = 5.11 ± 2.16 mmol/kg; data not shown; Johannesson et al., 2005). The groundwaters are Na–Ca–HCO_3 type waters (Johannesson et al., 2005). Dissolved REE concentrations are similar to other circumneutral pH groundwaters and within the range reported for modern seawater (Bertram and Elderfield, 1993; Johannesson et al., 1997; Tang and Johannesson, 2005).

Table 5
Shale-normalized Ce, Pr, and Gd anomalies, molal Y/Ho ratios, and shale-normalized La/Yb, Pr/Yb, Nd/Yb, and Gd/Yb ratios for groundwaters from León Valley, Guanajuato and from the city of Querétaro in central México

	Ce/Ce^*	Pr/Pr^*	Gd/Gd^*	Y/Ho	La/Yb	Pr/Yb	Nd/Yb	Gd/Yb
León Valley								
Lagunillas	0.42	1.39	1.93	90.9	0.13	0.11	0.10	0.62
Ciudad 33	0.14	0.76	2.94	134	0.25	0.09	0.21	1.61
Ciudad 35	0.29	1.16	2.85	98.9	0.12	0.10	0.15	1.80
Ciudad 41	0.17	1.42	1.49	102	0.33	0.28	0.34	1.11
Oriente 4	0.16	1.16	1.76	113	0.26	0.16	0.25	0.84
Sur 8	0.23	1.07	1.13	114	0.30	0.16	0.24	0.57
Sur 11	0.09	1.31	2.31	100	0.36	0.24	0.34	1.54
Turbio B-1	0.40	0.97	2.51	150	0.27	0.17	0.25	0.97
Turbio 12	0.10	1.44	1.18	111	0.19	0.12	0.15	0.42
Turbio 14	0.12	1.42	1.37	88.6	0.50	0.42	0.54	1.10
Mean	0.21	1.21	1.95	110	0.27	0.18	0.26	1.06
SD	0.12	0.21	0.64	18.3	0.11	0.10	0.12	0.45
Median	0.17	1.23	1.85	106	0.26	0.16	0.24	1.04
Querétaro								
Capilla 1Bis	0.32	1.42	0.87	111	0.11	0.07	0.06	0.23
Capilla 2	0.26	1.34	0.72	90.2	0.05	0.05	0.06	0.17
Capilla 3	0.51	1.25	0.99	147	0.28	0.21	0.21	0.52
Capilla 6	0.44	1.18	1.64	106	0.12	0.08	0.08	0.49
Juriquilla-UNAM	0.29	1.42	1.06	135	0.25	0.21	0.23	0.71
Chichimequillas 2	0.23	2.04	1.87	96.5	0.26	0.18	0.13	0.78
San Isidro-Miranda	0.36	1.52	1.29	90.4	0.57	0.51	0.48	1.02
Salitre	0.12	1.11	0.90	89.4	0.03	0.02	0.03	0.19
Santa Rosa-Jaurequi	0.14	1.64	1.00	118	0.16	0.13	0.13	0.48
Expositor 1	0.16	1.61	0.92	85.0	0.07		0.08	0.27
Pueblito 3	0.27	1.41	1.01	115	0.07	0.06	0.06	0.17
Virreyes	0.24	1.89	0.55	104	0.16	0.11	0.09	0.20
La Negreta	0.07	1.28	0.84	84.2	0.02	0.03	0.05	0.20
San Miguelito	0.19	1.47	0.33	88.1	0.13	0.13	0.15	0.13
Alameda Park	0.30	1.52	0.28	86.7	0.02	0.02	0.02	0.03
Tlacote	0.57	1.13	0.68	88.1	0.18	0.17	0.20	0.35
Mompani	0.21	1.54	0.50	105	0.10	0.08	0.09	0.15
Mean	0.28	1.46	0.91	102	0.15	0.13	0.13	0.36
SD	0.13	0.24	0.40	17.8	0.13	0.11	0.11	0.26
Median	0.26	1.42	0.90	96.5	0.12	0.08	0.09	0.23

See Table 1 for details.

Shale-normalized REE patterns for groundwaters from the León Valley of Guanajuato and the region surrounding the city of Querétaro in central México are shown in Figs. 7 and 8, respectively. Groundwater REE concentrations are normalized to PAAS in order to be consistent with the PAAS-normalized REE patterns for seawater and chemical sediment data presented in Figs. 1–5. The outstanding feature of the REE patterns of León Valley and Querétaro groundwaters is their general similarities to modern seawater, GBR coral and microbial carbonates, and Archean chemical sediments (compare Figs. 7 and 8 with Figs. 1–5). All of the groundwater samples exhibit substantial negative Ce anomalies and enrichments in the HREEs relative to the LREEs (Table 5). Moreover, the majority of the groundwaters have enrichments in La (i.e., positive La-anomalies) compared to their shale-normalized values for Pr and Nd (Figs. 7–9). The resulting positive shale-normalized La-anomalies, as defined by Bau and Dulski (1996), closely resemble those of modern seawater (Fig. 9). The León and Querétaro groundwaters also have superchrondritic Y anomalies (mean values of 110 and 102, respectively; Table 5), which are again similar in magnitude to those reported for modern seawater (e.g., mean = 108; Nozaki et al., 1997).

4.2. Statistical results

Results of the statistical comparisons of Ce, Gd, and Y anomalies and measures of HREE enrichment for modern seawater, groundwater, and chemical sediments (Tables 1–3 and 5) are presented in the appendix (Table A1) for both the ANOVA and Wilcoxon methods. In general, the statistical results mirror the readily observable similarities and differences in the REE patterns. For example, the presence of Ce anomalies in seawater patterns and their absence in Archean chemical sediment REE plots are reflected in the corresponding p values (Table A1).

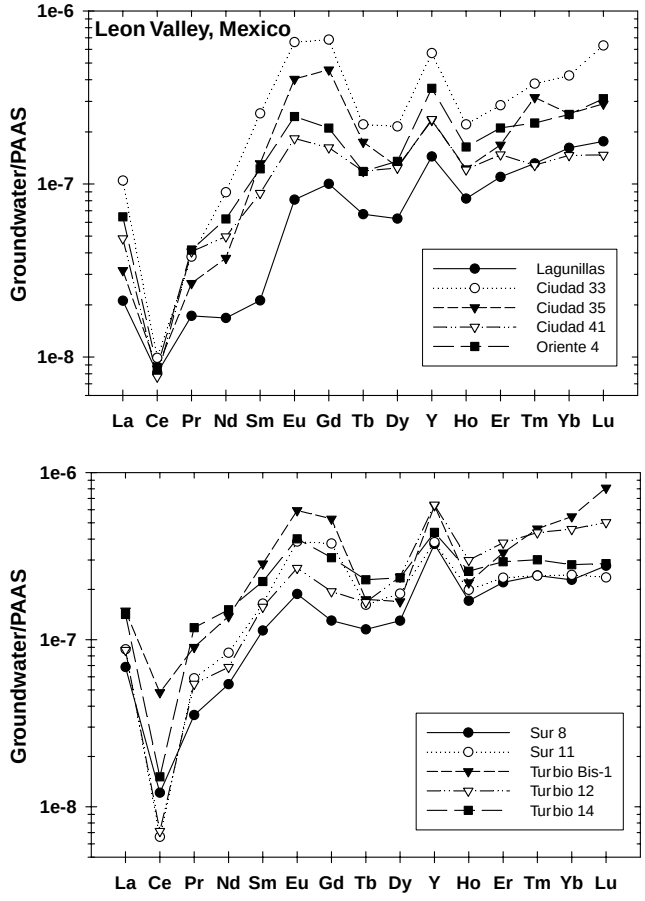

Fig. 7. Shale-normalized REE + Y patterns of groundwater samples from the León Valley surrounding León, Guanajuato, México.

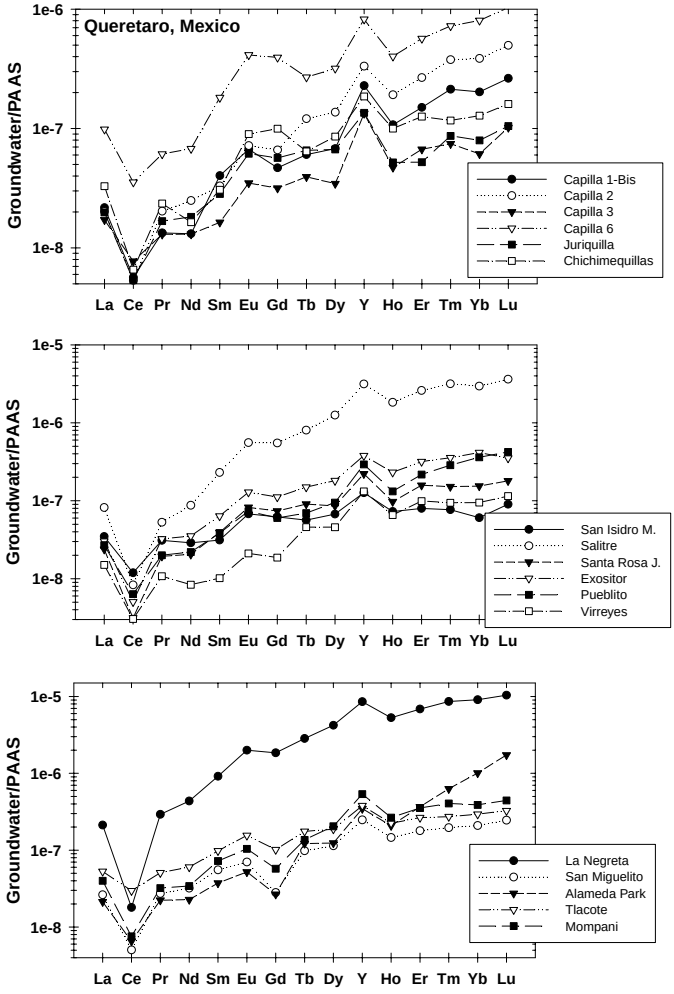

Fig. 8. Shale-normalized REE + Y patterns of groundwater samples from the region surrounding the city of Querétaro in Querétaro, México.

The statistical analysis also reveals subtle differences between the Holocene microbialites and modern seawater (e.g., Ce/Ce*, Y/Ho, LREE/HREE ratios). Moreover, REE patterns of the Archean chemical sediments differ significantly from open-ocean and ocean-margin seawater in terms of Gd anomalies, Y/Ho ratios, and measures of REE enrichment, in addition to Ce and Eu anomalies (Table A1). León Valley groundwaters have REE patterns that are statistically indistinguishable from those of open-ocean seawater in terms of Ce anomalies, Y/Ho ratios, and measures of REE fractionation; whereas REE patterns for Querétaro groundwaters are more similar to shoreline/enclosed bay seawater (Table A1). Statistical comparisons of the REE patterns of the groundwaters to those of the Archean chemical sediments also reveal important similarities. With the exception of Ce anomalies, León Valley groundwaters have REE patterns that are statistically indistinguishable from the laminated sediments of the Strelley Pool Chert, and Querétaro groundwaters only differ from the stromatolitic Strelley Pool Chert samples in terms of Ce and Gd anomalies, and by Ce anomalies and $(Gd/Yb)_{SN}$ ratios for the laminated sediments (Table A1).

5. Discussion

5.1. Seawater and terrestrial water REE patterns

Previous investigations demonstrate that many river waters, groundwaters, and some lake waters exhibit HREE enriched fractionation patterns similar to those of modern seawater (e.g., Elderfield et al., 1990; Smedley, 1991; Johannesson and Lyons, 1994; Sholkovitz, 1995; Johannesson et al., 1999; Johannesson and Hendry, 2000). Furthermore, it is generally agreed that the HREE enriched patterns of modern seawater actually begin forming on the continents during chemical weathering and riverine transport of dissolved REEs to the oceans (Hoyle et al., 1984; Goldstein and Jacobsen, 1988; Elderfield et al., 1990; Byrne and Liu, 1998). Comparison of the Ce, Pr, and Gd anomalies (0.59, 1.04, and 1.23, respectively) and $(La/Yb)_{SN}$, $(Pr/Yb)_{SN}$, $(Nd/Yb)_{SN}$, and $(Gd/Yb)_{SN}$ ratios (0.21, 0.12, 0.25, and 0.65, respectively, where SN = PAAS; median values for $n = 21$) of waters of the Rhine and its upper basin tributaries (see Fig. 9 of Tricca et al., 1999) with those of modern seawater

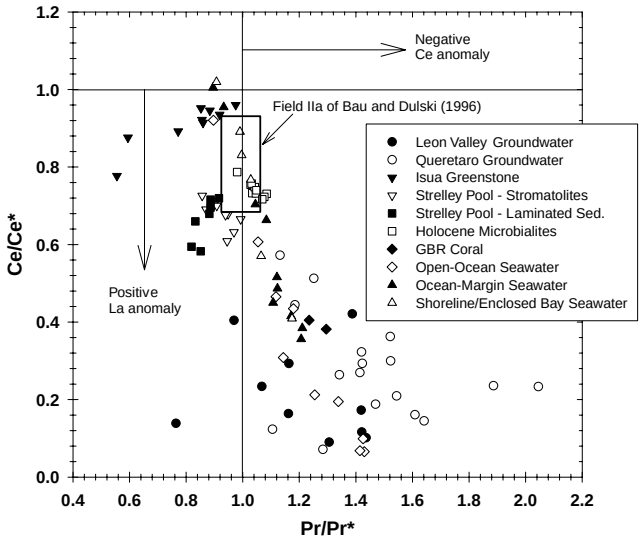

Fig. 9. Plot of the Ce anomaly (Ce/Ce^*) vs the Pr anomaly (Pr/Pr^*) for modern seawater, Holocene microbialite, modern reef coral, Strelley Pool Chert, Isua Greenstone Belt BIFs, and groundwaters from León Valley and Querétaro, México. The diagram is after Bau and Dulski (1996) and is used to discriminate La and Ce anomalies. Field II a shows region were samples with positive La anomalies and no Ce anomalies plot (Bau and Dulski, 1996).

(Table 1) illustrates the similarities of the respective REE patterns. Although the degree of fractionation is commonly less substantial in river waters compared to seawater, the general processes that act to fractionate REEs in the oceans (e.g., solution and surface complexation reactions; Elderfield et al., 1990; Sholkovitz, 1995; Byrne and Liu, 1998; Quinn et al., 2004) also clearly operate in terrestrial waters.

The seawater-like REE patterns of León Valley and Querétaro groundwaters (Figs. 7 and 8) provide further evidence that terrestrial waters can have REE patterns that resemble those of modern seawater. Moreover, the statistical comparisons of REE patterns of these central México groundwaters to those of modern seawater quantitatively demonstrate the resemblance of the respective REE patterns (Table A1). Specifically, the REE patterns of León Valley groundwaters are statistically indistinguishable from those of open-ocean seawater in terms of Ce anomalies, Y/Ho ratios, and $(La/Yb)_{SN}$, $(Pr/Yb)_{SN}$, and $(Nd/Yb)_{SN}$ ratios. In addition, the p value (i.e., 0.0065) for comparison of $(Gd/Yb)_{SN}$ ratios of León Valley groundwaters and open-ocean seawater is close to the 95% confidence interval cut-off ($p = 0.0071$). With the exception of differences in Ce/Ce^* and Gd/Gd^*, and Ce/Ce^* and Y/Ho ratios, respectively, the REE patterns of León Valley groundwater are also statistically indistinguishable from ocean-margin and shoreline/enclosed bay seawater REE patterns (Table A1). Querétaro groundwater REE patterns generally differ from those of seawater in terms of the degree of fractionation (i.e., comparatively less enriched in HREEs than seawater). Nonetheless, they also share many features of their REE patterns in common with those of seawater (Table A1). Consequently, careful analysis of natural terrestrial waters undeniably illustrates that features that are commonly considered to characterize modern seawater REE patterns (i.e., Ce and Gd anomalies, superchondritic Y/Ho ratios, enrichments in HREEs relative to LREEs) are not unique to marine waters. Hence, to reiterate the findings of previous studies of rivers and groundwaters, those processes that fractionate REEs in the oceans (i.e., solution and surface complexation reactions that act to enhance input-normalized HREE concentrations compared to LREE, differential filling of the 4f electron shell that contributes to anomalously high La and Gd concentrations relative to neighboring REEs, and abiotic and/or biologically mediated Ce oxidation) also operate in terrestrial waters, leading to REE patterns that closely resemble those of seawater (e.g., Elderfield et al., 1990; Byrne and Liu, 1998; Johannesson et al., 1999, 2005; Johannesson and Hendry, 2000). Accordingly, ancient chemical sediments that possess REE distribution patterns resembling those of modern seawater may not necessarily have formed in a marine environment as a terrestrial setting would seem equally plausible.

5.2. Groundwater and Archean chemical sediment REE patterns

Numerous studies discuss the paleo-oceanographic implications of the general similarities between the shale-normalized REE patterns of ancient chemical sediments such as BIFs and those of modern seawater (e.g., Appel, 1983; Derry and Jacobsen, 1990; Shimizu et al., 1990; Danielson et al., 1992; Bau and Möller, 1993; Bau and Dulski, 1996; Yamamoto et al., 2004). Visual inspection of the shale-normalized REE plots of modern seawater (Figs. 1 and 2) and the Archean Strelley Pool Chert and Isua Greenstones (Figs. 4 and 5) clearly indicate similarities as well as differences. Comparison of the REE patterns of these Archean chemical sediments with those for León Valley and Querétaro groundwaters (Figs. 7 and 8) also reveal many similarities as well as differences. A noteworthy result of the statistical analysis is that the REE patterns of the Strelley Pool Chert are generally more similar to the REE patterns of the central México groundwaters than they are to those of modern seawater (Table A1). The resemblance is especially apparent between the laminated sediments of the Strelley Pool Chert and the groundwater samples.

The close likeness of Strelley Pool Chert and the shoreline/enclosed bay seawater REE patterns is consistent with formation of these rocks in a shallow, near-shore marine setting (e.g., Van Kranendonk et al., 2003). However, the statistical comparisons of the Strelley Pool Chert REE patterns with those of the central México groundwaters suggest that these Archean rocks

are just as likely to have formed in a groundwater (i.e., terrestrial) dominated environment as within a marine environment. Although the relatively well preserved sedimentary features of the Strelley Pool Chert support formation within a shallow marine or intertidal environment, in their absence, such a conclusion would be equivocal if based only on the REE data. Furthermore, some of the sedimentary features reported to occur within the Strelley Pool Chert are also consistent with structures found in modern groundwater discharge zones along the arid coastlines of Arabia and Persia (i.e., sabkhas; Butler, 1969; Kinsman, 1969; Patterson and Kinsman, 1982; Ferguson and Skyring, 1995). Hence, whereas we agree with Van Kranendonk et al. (2003) that the REE data are consistent with formation of the Archean Strelley Pool Chert within a sabkha setting, in contrast to these researchers who suggest formation of these Archean rocks in a shallow, peritidal setting, we point out that modern coastal sabkhas are groundwater-dominated, supratidal environments and not peritidal, marine-dominated systems (Kinsman, 1969;Wood et al., 2002; Yechieli and Wood, 2002). Therefore, groundwater with REE patterns like those of León Valley and/or Querétaro, discharging to an Archean coastal sabkha seems as likely a source for the REE distribution patterns of Strelley Pool Chert samples as the Archean shallow marine (i.e., peritidal) origin discussed by Van Kranendonk et al. (2003). Investigation of REEs in modern coastal sabkhas is, however, necessary to test this hypothesis.

Neglecting the obvious differences in Ce and Eu anomalies, BIFs of the Isua Greenstone Belt are generally similar to modern seawater in terms of their overall REE patterns. However, close inspection and, in particular, the statistical analysis, also reveal important differences between Isua rocks and modern seawater REE patterns, and similarities between the REE patterns of these rocks and the central México groundwaters (Table A1). Additionally, Fig. 9 demonstrates that modern seawater, GBR corals, and the groundwaters from central México have identical shale-normalized La anomalies, whereas the Isua BIFs, Strelley Pool Chert, and Holocene microbialites have significantly smaller La anomalies, or plot within the region where samples do not exhibit La anomalies (Bau and Dulski, 1996). Moreover, many of the Holocene microbialite samples fall within the region defined by Bau and Dulski (1996) as having analytically insignificant Ce anomalies (Fig. 9; field IIa). Consequently, the REE patterns of the Isua Greenstone Belt BIFs also do not unequivocally support a marine environment for the formation of these Archean rocks. Indeed, based on the REE data, it is equally plausible that the BIFs of the Isua Greenstone Belt could have been influenced by terrestrial waters with REE distributions like groundwaters of the León Valley and the region surrounding the city of Querétaro.

6. Conclusions

Similarities in shale-normalized REE patterns of Archean chemical sediments and modern seawater are commonly cited as evidence for a marine origin of these ancient sedimentary rocks. More recently, resemblance of the REE patterns of Archean chemical sediments and Holocene reefal microbialites has been invoked in support of microbial facilitated mineral precipitation in Archean oceans. However, it is well known that natural waters from terrestrial settings (i.e., continental waters), including rivers and groundwaters, can also exhibit seawater-like REE patterns. Indeed, the HREE enriched pattern of modern seawater originates, in part, as a result of biogeochemical processes/reactions occurring on the continents (Elderfield et al., 1990; Byrne and Liu, 1998). We present REE data for groundwaters from central México that also have seawater-like REE patterns, and apply statistical techniques to quantitatively compare the variance in REE patterns for modern seawater, Archean chemical sediments, and terrestrial waters (i.e., groundwaters from central México). Visual inspection and statistical analysis of shale-normalized REE patterns indicate strong similarities between seawater, Archean chemical sediments, and terrestrial waters, underscoring the results of earlier investigations (e.g,. Elderfield et al., 1990; Sholkovitz, 1995). Consequently, in the absence of well preserved sedimentary structures and/or Nd isotopic data, it is equivocal, at best, to conclude that Archean chemical sediments record the REE signature of Archean oceans. Furthermore, our analysis illustrates that seawater-like REE patterns of Archean chemical sediments do not definitively demonstrate that such rocks formed as a result of microbial processes in an Archean ocean.

Acknowledgments

This work was supported in part by NSF Grant INT-9912159 to K. Johannesson and CEAS-XXVI-OD-UNAM-99-088 to A. Cortés and K. Johannesson. We are especially grateful to Ing. José Luis Cruz José, project director at the Comision Estatal de Agua y Saneamiento de Guanajuato for his interest in this project, for access to the wells, and for assistance with sampling. We thank Dr. José A. Ramos Leal, Ms. Adina Rose, and Mr. Alejandro G. Ramírez for assistance with sample collection. Discussions with Dr. Jianwu Tang and Ms. Shama Haque greatly improved the manuscript. We thank Drs. Z. Chen and C. Jones of Old Dominion University for ICP-MS analysis. The manuscript benefitted greatly from the comments of three anonymous reviewers, and those of the associate editor, Dr. R.H. Byrne.

Associate editor: Robert H. Byrne

Appendix A

See Table A1.

Table A1
Statistical comparisons (ANOVA and Wilcoxon) of feature of shale-normalized REE patterns of seawater, groundwater from central México, Holocene microbialites, and Archean chemical sediments

Population 1	Population 2	Variable	ANOVA	Wilcoxon
Open ocean seawater	Ocean margin (coastal)	Ce/Ce^*	0.0372	0.0312
		Gd/Gd^*	0.6264	0.5317
		Y/Ho	0.1198	0.1629
		$(La/Yb)_{SN}$	0.4299	0.2787
		$(Pr/Yb)_{SN}$	0.2539	0.4272
		$(Nd/Yb)_{SN}$	0.1043	0.2081
		$(Gd/Yb)_{SN}$	0.1619	0.3055
Open ocean seawater	Enclosed bays (includes shoreline)	Ce/Ce^*	0.0079	0.0262
		Gd/Gd^*	***0.0061***	0.0253
		Y/Ho	***0.0065***	***0.0069***
		$(La/Yb)_{SN}$	0.0819	0.0635
		$(Pr/Yb)_{SN}$	0.8859	0.704
		$(Nd/Yb)_{SN}$	0.9742	0.7728
		$(Gd/Yb)_{SN}$	0.9163	0.9671
Open ocean seawater	León Valley	Ce/Ce^*	0.208	0.4274
		Gd/Gd^*	***0.0014***	***0.0009***
		Y/Ho	0.854	0.7133
		$(La/Yb)_{SN}$	0.8946	0.7035
		$(Pr/Yb)_{SN}$	0.4585	0.2121
		$(Nd/Yb)_{SN}$	0.9481	0.9766
		$(Gd/Yb)_{SN}$	***0.0011***	***0.0065***
Open ocean seawater	Querétaro	Ce/Ce^*	0.4485	0.94
		Gd/Gd^*	0.2193	0.0177
		Y/Ho	0.4745	0.3885
		$(La/Yb)_{SN}$	***0.0027***	***0.0003***
		$(Pr/Yb)_{SN}$	0.0404	***0.0053***
		$(Nd/Yb)_{SN}$	***0.0008***	***0.0005***
		$(Gd/Yb)_{SN}$	0.0207	0.0163
Open ocean seawater	Holocene microbialites	Ce/Ce^*	***0.0002***	***0.0028***
		Gd/Gd^*	0.1842	0.1779
		Y/Ho	0.7787	0.1779
		$(La/Yb)_{SN}$	***0.0000***	***0.0002***
		$(Pr/Yb)_{SN}$	0.414	0.5204
		$(Nd/Yb)_{SN}$	0.4449	0.93
		$(Gd/Yb)_{SN}$	0.7715	0.7474
Open ocean seawater	Modern reef coral	Ce/Ce^*	0.7883	0.7473
		Gd/Gd^*	—	—
		Y/Ho	0.6013	0.9062
		$(La/Yb)_{SN}$	0.0817	0.1513
		$(Pr/Yb)_{SN}$	0.9607	1.0
		$(Nd/Yb)_{SN}$	0.285	0.2472
		$(Gd/Yb)_{SN}$	0.8285	0.9577
Open ocean seawater	Strelley pool stromatolites	Ce/Ce^*	***0.0011***	***0.0028***
		Gd/Gd^*	***0.0000***	***0.0005***
		Y/Ho	0.0705	0.0792
		$(La/Yb)_{SN}$	***0.0000***	***0.0001***
		$(Pr/Yb)_{SN}$	***0.0000***	***0.0002***
		$(Nd/Yb)_{SN}$	***0.0000***	***0.0001***
		$(Gd/Yb)_{SN}$	0.1221	0.6606
Open ocean seawater	Strelley pool laminated	Ce/Ce^*	0.0078	0.0128
		Gd/Gd^*	***0.0003***	***0.0043***
		Y/Ho	0.4984	0.4587
		$(La/Yb)_{SN}$	***0.0029***	0.0125
		$(Pr/Yb)_{SN}$	***0.0011***	0.0072
		$(Nd/Yb)_{SN}$	***0.0046***	***0.0052***
		$(Gd/Yb)_{SN}$	0.0282	0.0571
Open ocean seawater	Isua Greenstone	Ce/Ce^*	***0.0000***	***0.0009***
		Gd/Gd^*	***0.0000***	***0.0004***
		Y/Ho	***0.0008***	***0.0004***
		$(La/Yb)_{SN}$	0.9795	0.5083
		$(Pr/Yb)_{SN}$	0.1219	0.2362
		$(Nd/Yb)_{SN}$	***0.0034***	***0.0004***
		$(Gd/Yb)_{SN}$	***0.0000***	***0.0001***
Ocean margin (coastal)	Enclosed bays (includes shoreline)	Ce/Ce^*	0.2123	0.2123
		Gd/Gd^*	***0.0014***	0.0138
		Y/Ho	***0.0005***	0.0085
		$(La/Yb)_{SN}$	0.2658	0.1158
		$(Pr/Yb)_{SN}$	0.2554	0.1752
		$(Nd/Yb)_{SN}$	0.1931	0.1431
		$(Gd/Yb)_{SN}$	0.2812	0.1158
Ocean margin (coastal)	León Valley	Ce/Ce^*	***0.0002***	***0.0008***
		Gd/Gd^*	***0.0027***	***0.0006***
		Y/Ho	0.0429	0.0685
		$(La/Yb)_{SN}$	0.7808	0.7913
		$(Pr/Yb)_{SN}$	0.1294	0.0539
		$(Nd/Yb)_{SN}$	0.3419	0.162
		$(Gd/Yb)_{SN}$	0.0111	0.0452
Ocean margin (coastal)	Querétaro	Ce/Ce^*	***0.0001***	***0.0005***
		Gd/Gd^*	0.2163	0.0133
		Y/Ho	0.2253	0.2812
		$(La/Yb)_{SN}$	0.0224	***0.0039***
		$(Pr/Yb)_{SN}$	***0.007***	***0.0006***
		$(Nd/Yb)_{SN}$	***0.0001***	***0.0002***
		$(Gd/Yb)_{SN}$	***0.0047***	***0.0046***
Ocean margin (coastal)	Holocene microbialites	Ce/Ce^*	0.0591	0.0258
		Gd/Gd^*	0.247	0.3509
		Y/Ho	***0.003***	***0.0067***
		$(La/Yb)_{SN}$	***0.0001***	***0.0008***
		$(Pr/Yb)_{SN}$	0.0127	0.014
		$(Nd/Yb)_{SN}$	***0.0028***	***0.0036***
		$(Gd/Yb)_{SN}$	0.0412	0.0757
Ocean margin (coastal)	Modern reef coral	Ce/Ce^*	0.2683	0.1626
		Gd/Gd^*	—	—
		Y/Ho	0.489	0.5139
		$(La/Yb)_{SN}$	0.2715	0.426
		$(Pr/Yb)_{SN}$	0.5093	0.7473
		$(Nd/Yb)_{SN}$	0.0112	0.0169
		$(Gd/Yb)_{SN}$	0.0896	0.1039
Ocean margin (coastal)	Strelley pool stromatolites	Ce/Ce^*	0.2647	0.1405
		Gd/Gd^*	***0.0000***	***0.0005***
		Y/Ho	***0.0018***	***0.0067***
		$(La/Yb)_{SN}$	***0.0000***	***0.0002***
		$(Pr/Yb)_{SN}$	***0.0000***	***0.0002***
		$(Nd/Yb)_{SN}$	***0.0000***	***0.0002***
		$(Gd/Yb)_{SN}$	0.4173	0.9097
Ocean margin (coastal)	Strelley pool laminated	Ce/Ce^*	0.4487	0.2225
		Gd/Gd^*	***0.0004***	***0.0022***
		Y/Ho	0.0256	0.0933
		$(La/Yb)_{SN}$	0.0248	0.0218
		$(Pr/Yb)_{SN}$	***0.0000***	***0.0011***
		$(Nd/Yb)_{SN}$	***0.0002***	***0.0054***
		$(Gd/Yb)_{SN}$	0.1254	0.1877

(continued on next page)

Table A1 (*continued*)

Population 1	Population 2	Variable	ANOVA	Wilcoxon
Ocean margin (coastal)	Isua Greenstone	Ce/Ce^*	***0.001***	0.0247
		Gd/Gd^*	***0.0000***	***0.0006***
		Y/Ho	***0.0006***	***0.0033***
		$(La/Yb)_{SN}$	0.8471	0.5956
		$(Pr/Yb)_{SN}$	0.2162	0.5403
		$(Nd/Yb)_{SN}$	0.0312	***0.0062***
		$(Gd/Yb)_{SN}$	***0.0005***	***0.0003***
Enclosed bays (includes shoreline)	León Valley	Ce/Ce^*	***0.0000***	***0.002***
		Gd/Gd^*	0.0536	0.0562
		Y/Ho	***0.0011***	***0.0058***
		$(La/Yb)_{SN}$	0.3624	0.4159
		$(Pr/Yb)_{SN}$	0.6195	0.4159
		$(Nd/Yb)_{SN}$	0.9483	0.7823
		$(Gd/Yb)_{SN}$	0.0279	0.0262
Enclosed bays (includes shoreline)	Querétaro	Ce/Ce^*	***0.0000***	***0.0011***
		Gd/Gd^*	0.1745	0.0542
		Y/Ho	***0.0017***	***0.0027***
		$(La/Yb)_{SN}$	0.2729	0.0999
		$(Pr/Yb)_{SN}$	0.1221	0.0229
		$(Nd/Yb)_{SN}$	0.0189	***0.007***
		$(Gd/Yb)_{SN}$	0.096	0.0542
Enclosed bays (includes shoreline)	Holocene microbialites	Ce/Ce^*	0.9341	0.3566
		Gd/Gd^*	***0.005***	0.0284
		Y/Ho	***0.0000***	***0.0058***
		$(La/Yb)_{SN}$	0.2072	0.5508
		$(Pr/Yb)_{SN}$	0.5856	1.0
		$(Nd/Yb)_{SN}$	0.5452	0.8708
		$(Gd/Yb)_{SN}$	0.9067	0.4159
Enclosed bays (includes shoreline)	Modern reef coral	Ce/Ce^*	0.0764	0.0668
		Gd/Gd^*	—	—
		Y/Ho	***0.0004***	0.1052
		$(La/Yb)_{SN}$	0.9432	0.7842
		$(Pr/Yb)_{SN}$	0.8986	0.8676
		$(Nd/Yb)_{SN}$	0.4051	0.5228
		$(Gd/Yb)_{SN}$	0.7902	1.0
Enclosed bays (includes shoreline)	Strelley pool stromatolites	Ce/Ce^*	0.3437	0.3028
		Gd/Gd^*	0.1985	0.1376
		Y/Ho	***0.0006***	***0.0058***
		$(La/Yb)_{SN}$	0.0089	0.0147
		$(Pr/Yb)_{SN}$	***0.0000***	***0.0014***
		$(Nd/Yb)_{SN}$	***0.0002***	***0.0014***
		$(Gd/Yb)_{SN}$	0.317	0.9568
Enclosed bays (includes shoreline)	Strelley pool laminated	Ce/Ce^*	0.3513	0.3531
		Gd/Gd^*	0.2167	0.1564
		Y/Ho	***0.0031***	0.0107
		$(La/Yb)_{SN}$	0.4245	0.3531
		$(Pr/Yb)_{SN}$	***0.0063***	0.0124
		$(Nd/Yb)_{SN}$	0.0343	0.0268
		$(Gd/Yb)_{SN}$	0.1471	0.0742
Enclosed bays (includes shoreline)	Isua Greenstone	Ce/Ce^*	0.0562	0.0875
		Gd/Gd^*	***0.0000***	***0.0069***
		Y/Ho	0.2093	0.2472
		$(La/Yb)_{SN}$	0.5765	0.953
		$(Pr/Yb)_{SN}$	0.2159	0.4437
		$(Nd/Yb)_{SN}$	0.0494	0.0157
		$(Gd/Yb)_{SN}$	***0.0029***	0.0113
León Valley	Querétaro	Ce/Ce^*	0.2344	0.1834
		Gd/Gd^*	***0.0000***	***0.0002***
		Y/Ho	0.3008	0.2004
		$(La/Yb)_{SN}$	0.027	0.0084
		$(Pr/Yb)_{SN}$	0.205	0.0747
		$(Nd/Yb)_{SN}$	0.0096	***0.0028***
		$(Gd/Yb)_{SN}$	***0.0000***	***0.0004***
León Valley	Holocene microbialites	Ce/Ce^*	***0.0000***	***0.0002***
		Gd/Gd^*	***0.0011***	***0.0006***
		Y/Ho	0.5354	0.9699
		$(La/Yb)_{SN}$	0.0209	0.064
		$(Pr/Yb)_{SN}$	0.7289	0.1859
		$(Nd/Yb)_{SN}$	0.615	0.9699
		$(Gd/Yb)_{SN}$	***0.0043***	0.0113
León Valley	Modern reef coral	Ce/Ce^*	0.0724	0.1626
		Gd/Gd^*	—	—
		Y/Ho	0.4498	0.5912
		$(La/Yb)_{SN}$	0.4122	0.436
		$(Pr/Yb)_{SN}$	0.6979	0.3337
		$(Nd/Yb)_{SN}$	0.5062	0.5814
		$(Gd/Yb)_{SN}$	0.0538	0.0562
León Valley	Strelley pool stromatolites	Ce/Ce^*	***0.0000***	***0.0002***
		Gd/Gd^*	***0.0048***	0.0173
		Y/Ho	0.0645	0.1041
		$(La/Yb)_{SN}$	***0.0008***	***0.0028***
		$(Pr/Yb)_{SN}$	***0.0062***	***0.0004***
		$(Nd/Yb)_{SN}$	***0.0023***	***0.0013***
		$(Gd/Yb)_{SN}$	0.0977	0.162
León Valley	Strelley pool laminated	Ce/Ce^*	***0.0000***	***0.0008***
		Gd/Gd^*	0.0222	0.0359
		Y/Ho	0.5482	0.5259
		$(La/Yb)_{SN}$	0.0867	0.1074
		$(Pr/Yb)_{SN}$	0.0737	0.0359
		$(Nd/Yb)_{SN}$	0.0587	0.0454
		$(Gd/Yb)_{SN}$	0.3506	0.4068
León Valley	Isua Greenstone	Ce/Ce^*	***0.0000***	***0.0003***
		Gd/Gd^*	***0.0001***	***0.0003***
		Y/Ho	***0.0001***	***0.0003***
		$(La/Yb)_{SN}$	0.9711	0.5403
		$(Pr/Yb)_{SN}$	0.0781	0.0942
		$(Nd/Yb)_{SN}$	0.0189	***0.0038***
		$(Gd/Yb)_{SN}$	0.5522	0.7133
Querétaro	Holocene microbialites	Ce/Ce^*	***0.0000***	***0.0000***
		Gd/Gd^*	0.1277	***0.0062***
		Y/Ho	0.5225	0.2586
		$(La/Yb)_{SN}$	0.537	0.0747
		$(Pr/Yb)_{SN}$	0.0763	***0.0062***
		$(Nd/Yb)_{SN}$	***0.0051***	***0.0007***
		$(Gd/Yb)_{SN}$	0.0216	0.0072
Querétaro	Modern reef coral	Ce/Ce^*	0.2538	0.1631
		Gd/Gd^*	—	—
		Y/Ho	0.8065	1.0
		$(La/Yb)_{SN}$	0.2767	0.0848
		$(Pr/Yb)_{SN}$	0.3152	0.1631
		$(Nd/Yb)_{SN}$	0.0967	0.0344
		$(Gd/Yb)_{SN}$	0.2126	0.1941
Querétaro	Strelley pool stromatolites	Ce/Ce^*	***0.0000***	***0.0000***
		Gd/Gd^*	0.0145	***0.0024***
		Y/Ho	***0.003***	0.0084
		$(La/Yb)_{SN}$	0.4831	0.9001
		$(Pr/Yb)_{SN}$	0.2685	0.8605
		$(Nd/Yb)_{SN}$	0.6809	0.4074
		$(Gd/Yb)_{SN}$	***0.0056***	0.0097

Table A1 (*continued*)

Population 1	Population 2	Variable	ANOVA	Wilcoxon
Querétaro	Strelley pool laminated	Ce/Ce*	***0.0000***	***0.0002***
		Gd/Gd*	0.286	0.0076
		Y/Ho	0.125	0.253
		$(La/Yb)_{SN}$	0.6524	0.2803
		$(Pr/Yb)_{SN}$	0.6373	1.0
		$(Nd/Yb)_{SN}$	0.6636	0.204
		$(Gd/Yb)_{SN}$	***0.0023***	***0.0043***
Querétaro	Isua Greenstone	Ce/Ce*	***0.0000***	***0.0000***
		Gd/Gd*	0.2524	0.1778
		Y/Ho	***0.0002***	***0.0000***
		$(La/Yb)_{SN}$	0.0894	0.1181
		$(Pr/Yb)_{SN}$	0.0051	0.0025
		$(Nd/Yb)_{SN}$	***0.0000***	***0.0002***
		$(Gd/Yb)_{SN}$	***0.0000***	***0.0003***
Holocene microbialites	Modern reef coral	Ce/Ce*	***0.0000***	0.0413
		Gd/Gd*	—	—
		Y/Ho	0.1028	0.1071
		$(La/Yb)_{SN}$	0.1097	0.159
		$(Pr/Yb)_{SN}$	0.4131	0.9145
		$(Nd/Yb)_{SN}$	0.2817	0.1985
		$(Gd/Yb)_{SN}$	0.4156	0.2293
Holocene microbialites	Strelley pool stromatolites	Ce/Ce*	***0.0001***	***0.0003***
		Gd/Gd*	***0.0000***	***0.0004***
		Y/Ho	0.0102	0.089
		$(La/Yb)_{SN}$	***0.0004***	***0.0022***
		$(Pr/Yb)_{SN}$	***0.0000***	***0.0002***
		$(Nd/Yb)_{SN}$	***0.0000***	***0.0002***
		$(Gd/Yb)_{SN}$	***0.0000***	***0.0004***
Holocene microbialites	Strelley pool laminated	Ce/Ce*	***0.0009***	***0.0011***
		Gd/Gd*	***0.0003***	***0.004***
		Y/Ho	0.193	0.1571
		$(La/Yb)_{SN}$	0.9541	0.3539
		$(Pr/Yb)_{SN}$	***0.0000***	***0.004***
		$(Nd/Yb)_{SN}$	***0.0028***	0.0168
		$(Gd/Yb)_{SN}$	0.0508	***0.0054***
Holocene microbialites	Isua Greenstone	Ce/Ce*	***0.0000***	***0.0004***
		Gd/Gd*	***0.0000***	***0.0003***
		Y/Ho	***0.0000***	***0.0003***
		$(La/Yb)_{SN}$	0.1879	0.5956
		$(Pr/Yb)_{SN}$	0.0752	0.1309
		$(Nd/Yb)_{SN}$	***0.0065***	***0.0005***
		$(Gd/Yb)_{SN}$	***0.0000***	***0.0003***
Modern reef coral	Strelley pool stromatolites	Ce/Ce*	***0.0000***	0.0413
		Gd/Gd*	—	—
		Y/Ho	0.1346	0.1626
		$(La/Yb)_{SN}$	***0.0033***	0.0235
		$(Pr/Yb)_{SN}$	***0.0000***	0.0413
		$(Nd/Yb)_{SN}$	***0.0001***	***0.0027***
		$(Gd/Yb)_{SN}$	0.3323	1.0
Modern reef coral	Strelley pool laminated	Ce/Ce*	***0.0003***	0.057
		Gd/Gd*	—	—
		Y/Ho	0.3508	0.4642
		$(La/Yb)_{SN}$	0.3746	0.2556
		$(Pr/Yb)_{SN}$	0.0278	0.1074
		$(Nd/Yb)_{SN}$	0.1005	0.0513
		$(Gd/Yb)_{SN}$	0.1853	0.0726
Modern reef coral	Isua Greenstone	Ce/Ce*	***0.0000***	0.0451
		Gd/Gd*	—	—
		Y/Ho	***0.0045***	0.0451
		$(La/Yb)_{SN}$	0.6294	1.0
		$(Pr/Yb)_{SN}$	0.4996	0.5557
		$(Nd/Yb)_{SN}$	0.0407	***0.0051***
		$(Gd/Yb)_{SN}$	***0.0049***	***0.0069***
Strelley pool stromatolites	Strelley pool laminated	Ce/Ce*	0.4989	0.7327
		Gd/Gd*	0.527	0.4068
		Y/Ho	0.2813	0.2225
		$(La/Yb)_{SN}$	0.0863	0.057
		$(Pr/Yb)_{SN}$	0.1979	0.7327
		$(Nd/Yb)_{SN}$	0.1865	0.3055
		$(Gd/Yb)_{SN}$	0.549	0.5259
Strelley pool stromatolites	Isua Greenstone	Ce/Ce*	***0.0000***	***0.0003***
		Gd/Gd*	***0.0000***	***0.0003***
		Y/Ho	***0.0000***	***0.0003***
		$(La/Yb)_{SN}$	0.0423	0.1114
		$(Pr/Yb)_{SN}$	***0.0035***	***0.0013***
		$(Nd/Yb)_{SN}$	***0.0003***	***0.0003***
		$(Gd/Yb)_{SN}$	0.1283	0.2057
Strelley pool laminated	Isua Greenstone	Ce/Ce*	***0.0000***	***0.001***
		Gd/Gd*	***0.0000***	***0.001***
		Y/Ho	***0.0002***	***0.0021***
		$(La/Yb)_{SN}$	0.2913	0.5966
		$(Pr/Yb)_{SN}$	0.0235	***0.0059***
		$(Nd/Yb)_{SN}$	***0.005***	***0.0015***
		$(Gd/Yb)_{SN}$	0.5092	0.1123

Tabulated are two-sided p values from the indicated procedures. A result is statistically significant by the Bonferroni procedure if $p < 0.05/7 = 0.0071$ (shown in bold italics).

References

Appel, P.W.U., 1983. Rare earth elements in the Early Archaean Isua iron-formation, West Greenland. *Precambrian Res.* **20**, 243–258.

Barghoorn, E.S., Schopf, J.W., 1966. Microorganisms three billion years old from the Precambrian of South Africa. *Science* **152**, 758–763.

Bau, M., 1996. Controls on the fractionation of isovalent trace elements in magmatic and aqueous systems: evidence from Y/Ho, Zr/Hf, and lanthanide tetrad effect. *Contrib. Mineral. Petrol.* **123**, 323–333.

Bau, M., 1999. Scavenging of dissolved yttrium and rare earths by precipitating iron oxyhydroxide: experimental evidence for Ce oxidation, Y–Ho fractionation, and lanthanide tetrad effect. *Geochim. Cosmochim. Acta* **63**, 67–77.

Bau, M., Möller, P., 1993. Rare earth element systematics of the chemically precipitated component of Early Precambrian iron formations and the evolution of the terrestrial atmosphere–hydrosphere–lithosphere. *Geochim. Cosmochim. Acta* **57**, 2239–2249.

Bau, M., Dulski, P., 1996. Distribution of yttrium and rare-earth elements in the Penge and Kuruman iron-formations, Transvaal Supergroup, South Africa. *Precambrian Res.* **79**, 37–55.

Bau, M., Dulski, P., Möller, P., 1995. Yttrium and holmium in South Pacific seawater: vertical distribution and possible fractionation behavior. *Chem. Erde* **55**, 1–15.

Bau, M., Koschinsky, A., Dulski, P., Hein, J.R., 1996. Comparison of the partitioning behaviours of yttrium, rare earth elements, and titanium between hydrogenetic marine ferromanganese crusts and seawater. *Geochim. Cosmochim. Acta* **60**, 1709–1725.

Bertram, C.J., Elderfield, H., 1993. The geochemical balance of the rare earth elements an neodymium isotopes in the oceans. *Geochim. Cosmochim. Acta* **57**, 1957–1986.

Bolhar, R., Kamber, B.S., Moorbath, S., Fedo, C.M., Whitehouse, M.J., 2004. Characterisation of early Archaean chemical sediments by trace element signatures. *Earth Planet. Sci. Lett.* **222**, 43–60.

Bolhar, R., Van Kranendonk, M.J., Kamber, B.S., 2005. A trace element study of siderite-jasper banded iron formation in the 3.45 Ga Warrawoona Group, Pilbara Craton—formation from hydrothermal fluids and shallow seawater. *Precambrian Res.* **137**, 93–114.

Brasier, M.D., Green, O.R., Jephcoat, A.P., Kleppe, A.K., Van Kranendonk, M.J., Lindsay, J.F., Steele, A., Grassineau, N.V., 2002. Questioning the evidence for Earth's oldest fossils. *Nature* **416**, 76–81.

Butler, G.P., 1969. Modern evaporite deposition and geochemistry of coexisting brines, the sabkha, Trucial Coast, Arabian Gulf. *J. Sed. Petrol.* **39**, 70–89.

Byrne, R.H., Kim, K.-H., 1990. Rare earth element scavenging in seawater. *Geochim. Cosmochim. Acta* **54**, 2645–2656.

Byrne, R.H., Li, B., 1995. Comparative complexation behavior of the rare earths. *Geochim. Cosmochim. Acta* **59**, 4575–4589.

Byrne, R.H., Liu, X., 1998. A coupled riverine–marine fractionation model for dissolved rare earths and yttrium. *Aquatic Geochem.* **4**, 103–121.

Byrne, R.H., Liu, X., Schijf, J., 1996. The influence of phosphate coprecipitation on rare earth distributions in natural waters. *Geochim. Cosmochim. Acta* **60**, 3341–3346.

Cantrell, K.J., Byrne, R.H., 1987. Rare earth element complexation by carbonate and oxalate ions. *Geochim. Cosmochim. Acta* **51**, 597–605.

Danielson, A., Möller, P., Dulski, P., 1992. The europium anomalies in banded iron formation and the thermal history of the oceanic crust. *Chem. Geol.* **97**, 89–100.

Dauphas, N., van Zuilen, M., Wadhwa, M., Davis, A.M., Marty, B., Janney, P.E., 2004. Clues from Fe isotope variations of the origins of early Archean BIFs from Greenland. *Science* **306**, 2077–2080.

De Baar, H.J.W., Schijf, J., Byrne, R.H., 1991. Solution chemistry of the rare earth elements in seawater. *Eur. J. Solid State Inorg. Chem.* **28**, 357–373.

DeCarlo, E.H., Wen, X.-Y., Irving, M., 1998. The influence of redox reactions on the uptake of dissolved Ce by suspended Fe and Mn oxide particle. *Aquatic Geochem.* **3**, 357–392.

Derry, L.A., Jacobsen, S.B., 1990. The chemical evolution of Precambian seawater: evidence from REEs in banded iron formations. *Geochim. Cosmochim. Acta* **54**, 2965–2977.

Dia, A., Gruau, G., Olivié-Lauquet, G., Riou, C., Molénat, J., Curmi, P., 2000. The distribution of rare earth elements in groundwaters: assessing the role of source-rock composition, redox changes and colloidal particles. *Geochim. Cosmochim. Acta* **64**, 4131–4151.

Duncan, T., Shaw, T.J., 2003. The mobility of rare earth elements and redox sensitive elements in the groundwater/seawater mixing zone of a shallow coastal aquifer. *Aquatic Geochem.* **9**, 233–255.

Elderfield, H., 1988. The oceanic chemistry of the rare-earth elements. *Philos. Trans. R. Soc. London A* **325**, 105–126.

Elderfield, H., Greaves, M.J., 1982. The rare earth elements in seawater. *Nature* **296**, 214–219.

Elderfield, H., Pagett, R., 1986. Rare earth elements in ichthyoliths: variations with redox conditions and depositional environment. *Sci. Total Environ.* **49**, 175–197.

Elderfield, H., Upstill-Goddard, R., Sholkovitz, E.R., 1990. The rare earth elements in rivers, estuaries, and coastal seas and their significance to the composition of ocean waters. *Geochim. Cosmochim. Acta* **54**, 971–991.

Fedo, C.M., Whitehouse, M.J., 2002. Metasomatic origin of quartz-pyroxene rock, Akilia, Greenland, and implications for Earth's earliest life. *Science* **296**, 1448–1452.

Ferguson, J., Skyring, G.W., 1995. Redbed-associated sabkhas and tidal flats at Shark Bay, Western Australia: their significance for genetic models of stratiform Cu–(Pb–Zn) deposits. *Aust. J. Earth Sci.* **42**, 321–333.

Field, M.P., Sherrell, R.M., 1998. Magnetic sector ICPMS with desolvating micronebulization: interference-free subpicogram determination of rare earth elements in natural samples. *Anal. Chem.* **70**, 4480–4486.

Goldstein, S.J., Jacobsen, S.B., 1987. The Nd and Sr isotopic systematics of river-water dissolved material: implications for the sources of Nd and Sr in seawater. *Chem. Geol.* **66**, 245–272.

Goldstein, S.J., Jacobsen, S.B., 1988. Rare earth elements in river waters. *Earth Planet. Sci. Lett.* **89**, 35–47.

Grandjean, P., Cappetta, H., Michard, A., Albarède, F., 1987. The assessment of REE patterns and $^{143}Nd/^{144}Nd$ ratios in fish remains. *Earth Planet. Sci. Lett.* **84**, 181–196.

Hanson, G.N., 1980. Rare earth elements in petrogenetic studies of igneous systems. *Ann. Rev. Earth Planet. Sci.* **8**, 371–406.

Hodge, V.F., Stetzenbach, K.J., Johannesson, K.H., 1998. Similarities in the chemical composition of carbonate groundwaters and seawater. *Environ. Sci. Technol.* **32**, 2481–2486.

Høgdahl, O.T., Bowen, B.T., Melson, S., 1968. Neutron activation analysis of lanthanide elements in seawater. *Adv. Chem. Ser.* **73**, 308–325.

Hoyle, J., Elderfield, H., Gledhill, A., Greaves, M., 1984. The behaviour of the rare earth elements during the mixing of river and sea waters. *Geochim. Cosmochim. Acta* **48**, 143–149.

Johannesson, K.H., Lyons, W.B., 1994. The rare earth element geochemistry of Mono Lake water and the importance of carbonate complexing. *Limnol. Oceanogr.* **39**, 1141–1154.

Johannesson, K.H., Lyons, W.B., 1995. Rare-earth element geochemistry of Colour Lake, an acidic freshwater lake on Axel Heiberg Island, Northwest Territories, Canada. *Chem. Geol.* **119**, 209–223.

Johannesson, K.H., Hendry, M.J., 2000. Rare earth element geochemistry of groundwater from a thick till and clay-rich aquitard sequence, Saskatchewan, Canada. *Geochim. Cosmochim. Acta* **64**, 1493–1509.

Johannesson, K.H., Farnham, I.M., Guo, C., Stetzenbach, K.J., 1999. Rare earth element fractionation and concentration variations along a groundwater flow path within a shallow, basin-fill aquifer, southern Nevada, USA. *Geochim. Cosmochim. Acta* **63**, 2697–2708.

Johannesson, K.H., Cortés, A., Ramos Leal, J.A., Ramírez, A.G., Durazo, J., 2005. Geochemistry of rare earth elements in groundwaters from a rhyolite aquifer, central México. In: Johannesson, K.H. (Ed.), *Rare Earth Elements in Groundwater Flow Systems*. Springer, Dordrecht, pp. 187–222.

Johannesson, K.H., Stetzenbach, K.J., Hodge, V.F., Kreamer, D.K., Zhou, X., 1997. Delineation of ground-water flow systems in the southern Great Basin using aqueous rare earth element distributions. *Ground Water* **35**, 807–819.

Johannesson, K.H., Tang, J., Daniels, J.M., Bounds, W.J., Burdige, D.J., 2004. Rare earth element concentrations and speciation in organic-rich blackwaters of the Great Dismal Swamp, Virginia, USA. *Chem. Geol.* **209**, 271–294.

Kamber, B.S., Webb, G.E., 2001. The geochemistry of late Archaean microbial carbonate: implications for ocean chemistry and continental erosion history. *Geochim. Cosmochim. Acta* **65**, 2509–2525.

Kamber, B.S., Bolhar, R., Webb, G.E., 2004. Geochemistry of late Archaean stromatolites from Zimbabwe: evidence for microbial life in restricted epicontinental seas. *Precambrian Res.* **132**, 379–399.

Kim, K.-H., Byrne, R.H., Lee, J.H., 1991. Gadolinium behavior in seawater: a molecular basis for gadolinium anomalies. *Mar. Chem.* **36**, 107–120.

Kinsman, D.J.J., 1969. Modes of formation, sedimentary associations, and diagnostic features of shallow-water and supratidal evaporites. *AAPG Bull.* **53**, 830–840.

Klinkhammer, G., Elderfield, H., Hudson, A., 1983. Rare earth elements in seawater near hydrothermal vents. *Nature* **305**, 185–188.

Klinkhammer, G.P., Elderfield, H., Edmond, J.M., Mitra, A., 1994. Geochemical implications of rare earth element patterns in hydrothermal fluids from mid-ocean ridges. *Geochim. Cosmochim. Acta* **58**, 5105–5113.

Koeppenkastrop, D., DeCarlo, E.H., 1992. Sorption of rare earth elements from seawater onto synthetic mineral particles: an experimental approach. *Chem. Geol.* **95**, 251–263.

Koeppenkastrop, D., DeCarlo, E.H., 1993. Uptake of rare earth elements from solution by metal oxides. *Environ. Sci. Technol.* **27**, 1796–1806.

Lécuyer, C., Renyard, B., Grandjean, P., 2004. Rare earth element evolution of Phanerozoic seawater recorded in biogenic apatites. *Chem. Geol.* **204**, 63–102.

Leybourne, M.I., Goodfellow, W.D., Boyle, D.R., Hall, G.M., 2000. Rapid development of negative Ce anomalies in surface waters and contrasting REE patterns in groundwaters associated with Zn–Pb massive sulphide deposits. *Appl. Geochem.* **15**, 695–723.

McArthur, J.M., Walsh, J.N., 1984/1985. Rare-earth geochemistry of phosphorites. *Chem. Geol.* **47**, 191–220.

McKay, D.S., Gibson Jr, E.K., Thomas-Keprta, K.L., Vali, H., Romanek, C.S., Clemett, S.J., Chillier, X.D.F., Maechling, C.R., Zare, R.N., 1996. Search for past life on Mars: possible relic biogenic activity in Martian meteorite ALH84001. *Science* **273**, 924–930.

Miller, S.L., 1953. A production of amino acids under possible primitive Earth conditions. *Science* **117**, 528–529.

Moffett, J.W., 1990. Microbially mediated cerium oxidation in sea water. *Nature* **345**, 421–423.

Moffett, J.W., 1994. The relationship between cerium and manganese oxidization in the marine environment. *Limnol. Oceanogr.* **39**, 1309–1318.

Mojzsis, S.J., Arrhenius, G., McKeegan, K.D., Harrison, T.M., Nutman, A.P., Friend, C.R.L., 1996. Evidence for life on Earth before 3800 million years ago. *Nature* **384**, 55–59.

Möller, P., Dulski, P., Bau, M., 1994. Rare-earth element adsorption in a seawater profile above the East Pacific Rise. *Chem. Erde* **54**, 129–149.

Nance, W.B., Taylor, S.R., 1976. Rare earth element patterns and crustal evolution—I. Australian post-Archean sedimentary rocks. *Geochim. Cosmochim. Acta* **40**, 1539–1551.

Négrel, P.h., Guerrot, C., Cocherie, A., Azaroual, M., Brach, M., Fouillac, C.h., 2000. Rare earth elements, neodymium and strontium isotopic systematics in mineral waters: evidence from the Massif Central, France. *Appl. Geochem.* **15**, 1345–1367.

Nothdurft, L.D., Webb, G.E., Kamber, B.S., 2004. Rare earth element geochemistry of Late Devonian reefal carbonates, Canning Basin, Western Australia: confirmation of a seawater proxy in ancient limestones. *Geochim. Cosmochim. Acta* **68**, 263–283.

Nozaki, Y., Alibo, D.S., 2003. Importance of vertical geochemical processes in controlling the oceanic profiles of dissolved rare earth elements in the northeastern Indian Ocean. *Earth Planet. Sci. Lett.* **205**, 155–172.

Nozaki, Y., Zhang, J., 1995. The rare earth elements and yttrium in the coastal/offshore mixing zone of Tokyo Bat waters and the Kuroshio. In: Sakai, H., Nozaki, Y. (Eds.), *Biogeochemical Processes and Ocean Flux in the Western Pacific*. Terra Scientific Publishing, pp. 171–184.

Nozaki, Y., Zhang, J., Amakawa, H., 1997. The fractionation between Y and Ho in the marine environment. *Earth Planet. Sci. Lett.* **148**, 329–340.

Palmer, M.R., 1985. Rare earth elements in foraminifera tests. *Earth Planet. Sci. Lett.* **73**, 285–298.

Palmer, M.R., Elderfield, H., 1986. Rare earth elements and neodymium isotopes in ferromanganese oxide coatings pf Cenozoic foraminifera from the Atlantic Ocean. *Geochim. Cosmochim. Acta* **50**, 409–417.

Piepgras, D.J., Jacobsen, S.B., 1992. The behavior of rare earth elements in seawater: Precise determination of variations in the North Pacific water column. *Geochim. Cosmochim. Acta* **56**, 1851–1862.

Patterson, R.J., Kinsman, D.J.J., 1982. Formation of diagenetic dolomite in coastal sabkha along Arabian (Persian) Gulf. *AAPG Bull.* **66**, 28–43.

Piepgras, D.J., Wasserburg, G.J., 1987. Rare earth element transport in the western North Atlantic inferred from Nd isotopic observations. *Geochim. Cosmochim. Acta* **51**, 1257–1271.

Quinn, K.A., Byrne, R.H., Schijf, J., 2004. Comparative scavenging of yttrium and the rare earth elements in seawater: competitive influences of solution and surface complexataion. *Aquatic Geochem.* **10**, 59–80.

Reynard, B., Lécuyer, C., Grandjean, P., 1999. Crystal-chemical controls on rare earth element concentrations in fossil biogenic apatite and implications for paleoenvironmental reconstructions. *Chem. Geol.* **155**, 233–242.

Rosing, M.T., 1999. C-13-depleted carbon microparticles in >3700-Ma sea-floor sedimentary rocks from west Greenland. *Science* **283**, 674–676.

Schopf, J.W., 1993. Microfossils of the Early Archaean Apex Chert: new evidence for the antiquity of life. *Science* **260**, 640–646.

Schopf, J.W., Packer, B.M., 1987. Early Archaean (3.3 billion to 3.5 billion-year-old) microfossils from Warrawoona Group, Australia. *Science* **237**, 70–73.

Shannon, W.M., Wood, S.A., 2005. The analysis of picogram quantities of rare earth elements in natural waters. In: Johannesson, K.H. (Ed.), *Rare Earth Elements in Groundwater Flow Systems*. Springer, Dordrecht, pp. 1–37.

Shields, G., Stille, P., 2001. Diagenetic constraints on the use of cerium anomalies as palaeoseawater redox proxies: an isotopic and REE study of Cambrian phosphorites. *Chem. Geol.* **175**, 29–48.

Shields, G.A., Webb, G.E., 2004. Has the REE composition of seawater changed over geologic time. *Chem. Geol.* **204**, 103–107.

Shimizu, H., Umemoto, N., Masuda, A., Appel, P.W.U., 1990. Sources of iron-formations in the Archean Isua and Malene supracrustals, West Greenland: Evidence from La–Ce and Sm–Nd isotopic data and REE abundances. *Geochim. Cosmochim. Acta* **54**, 1147–1154.

Sholkovitz, E.R., 1995. The aquatic chemistry of rare earth elements in rivers and estuaries. *Aquatic Geochem.* **1**, 1–34.

Sholkovitz, E.R., Schneider, D.L., 1991. Cerium redox cycles and rare earth elements in the Sargasso Sea. *Geochim. Cosmochim. Acta* **55**, 2737–2743.

Sholkovitz, E.R., Shen, G.T., 1995. The incorporation of rare earth elements in modern coral. *Geochim. Cosmochim. Acta* **59**, 2749–2756.

Sholkovitz, E.R., Church, T.M., Arimoto, R., 1993. Rare earth element composition of precipitation, precipitation particles, and aerosols. *J. Geophys. Res.* **98**, 20587–20599.

Smedley, P.L., 1991. The geochemistry of rare earth elements in groundwater from the Carnmenellis area, southwest England. *Geochim. Cosmochim. Acta* **55**, 2767–2779.

Stetzenbach, K.J., Amano, M., Kreamer, D.K., Hodge, V.F., 1994. Testing the limits of ICP-MS: determination of trace elements in ground water at the parts-per-trillion level. *Ground Water* **32**, 976–985.

Tang, J., Johannesson, K.H., 2005. Rare earth element concentrations, speciation, and fractionation along groundwater flow paths: The Carrizo Sand (Texas) and Upper Floridan Aquifers. In: Johannesson, K.H. (Ed.), *Rare Earth Elements in Groundwater Flow Systems*. Springer, Dordrecht, pp. 223–251.

Taylor, S.R., 1964. Abundance of chemical elements in the continental crust: a new table. *Geochim. Cosmochim. Acta* **28**, 1273–1285.

Taylor, S.R., McLennan, S.M., 1985. *The Continental Crust: Its Composition and Evolution*. Blackwell, Oxford, 312 pp.

Tricca, A., Stille, P., Steinmann, M., Kiefel, B., Samuel, J., Eikenberg, J., 1999. Rare earth elements and Sr and Nd isotopic compositions of dissolved and suspended loads from small river systems in the Vosges mountains (France), the river Rhine and groundwater. *Chem. Geol.* **160**, 139–158.

Urey, H.C., 1952. On the early chemical history of the earth and the origins of life. *Proc. Natl. Acad. Sci. (U.S.)* **38**, 351–363.

Van Kranendonk, M.J., Webb, G.E., Kamber, B.S., 2003. Geological and trace element evidence for a marine sedimentary environment of deposition and biogenicity of 3.45 Ga stromatolitic carbonates in the Pilbara Craton, and support for a reducing Archean ocean. *Geobiology* **1**, 91–108.

Walter, M.R., Buick, R., Dunlop, J.S.R., 1980. Stromatolites, 3400–3500 Myr old from the North Pole area, Western Australia. *Nature* **284**, 443–445.

Webb, G.E., Kamber, B.S., 2000. Rare earth elements in Holocene reefal microbialites: A new shallow water proxy. *Geochim. Cosmochim. Acta* **64**, 1557–1565.

Westerlund, S., Öhman, P., 1992. Rare earth elements in the Arctic Ocean. *Deep-Sea Res.* **39**, 1613–1626.

Wood, W.W., Sanford, W.E., Al Habshi, A.R.S., 2002. Sources of solutes to the coastal sabkha of Abu Dhabi. *Geol. Soc. Am. Bull.* **114**, 259–268.

Wright, J., Schrader, H., Holser, W.T., 1987. Paleoredox variations in ancient oceans recorded by rare earth elements in fossil apatite. *Geochim. Cosmochim. Acta* **51**, 631–644.

Wyndham, T., McCulloch, M., Fallon, S., Alibert, C., 2004. High-resolution coral records of rare earth elements in coastal seawater: biogeochemical cycling and new environmental proxy. *Geochim. Cosmochim. Acta* **68**, 2067–2080.

Yamamoto, K., Itoh, N., Matsumoto, T., Tanaka, T., Adachi, M., 2004. Geochemistry of Precambian carbonate intercalated in pillows and its host basalt: implications for the REE composition of circa 3.4 Ga seawater. *Precambrian Res.* **135**, 331–344.

Yechieli, Y., Wood, W.W., 2002. Hydrogeologic processes in saline systems: playas, sabkhas, and saline lakes. *Earth-Sci. Rev.* **58**, 343–365.

Zhang, J., Nozaki, Y., 1996. Rare earth elements and yttrium in seawater: ICP-MS determinations in the East Caroline, Coral Sea, and South Fiji basins of the western South Pacific Ocean. *Geochim. Cosmochim. Acta* **60**, 4631–4644.

Zhang, J., Nozaki, Y., 1998. Behavior of rare earth elements in seawater at the ocean margin: a study along the slopes of the Sagami and Nankai troughs near Japan. *Geochim. Cosmochim. Acta* **62**, 1307–1317.

Zhang, Y.S., Amakawa, H., Nozaki, Y., 1994. The comparative behaviours of yttrium and lanthanides in the seawater of the North Pacific. *Geophys. Res. Lett.* **21**, 2677–2680.